Fatigue & Fracture of Engineering Materials & Structures

WILEY

FFEMS Fatigue & Fracture of Engineering Materials & Structures

INVITED REVIEW OPEN ACCESS

A Statistical Review of Hydrogen Effects on the Fatigue and Fracture Behavior of Steel

H. Wang[1] | N. O. Larrosa[2,3] | D. Engelberg[4] | R. Best[5] | L. Susmel[6]

[1]Department of Civil and Structural Engineering, The University of Sheffield, Sheffield, UK | [2]School of Electrical, Electronic and Mechanical Engineering, University of Bristol, Bristol, UK | [3]TECNALIA R&I, Basque Research and Technology Alliance (BRTA), Donostia-San Sebastián, Gipuzkoa, Spain | [4]Metallurgy and Corrosion, Department of Materials, The University of Manchester, Manchester, UK | [5]National Gas Transmission, UK | [6]Materials and Engineering Research Institute (MERI), Sheffield Hallam University, Sheffield, UK

Correspondence: L. Susmel (l.susmel@shu.ac.uk)

Received: 21 January 2025 | **Revised:** 22 April 2025 | **Accepted:** 10 May 2025

Funding: This work was supported by Engineering and Physical Sciences Research Council, EP/W524360/1; National Grid Gas Transmission.

Keywords: crack propagation | fatigue | hydrogen embrittlement | statistical analysis

ABSTRACT

This study conducts a statistical re-analysis of experimental data from the literature to assess the influence of hydrogen on key mechanical properties, including the medium-/high-cycle fatigue strength and the threshold value of the stress intensity factor range. The analysis employs linear regression, S-N curve plotting, and Paris' law regression. The results indicate that hydrogen has a minimal effect on the endurance limit of steel (estimated at 2×10^6 cycles to failure), in contrast to the reductions in lifespan observed in the medium-cycle fatigue regime. Regarding crack propagation, the threshold value of the stress intensity factor range is reduced in the presence of hydrogen, particularly in conventional steel, which is more susceptible to hydrogen embrittlement than stainless steel. Conversely, systematic evaluation of constants linked to Paris' equation across various material types revealed considerable variability, suggesting a non-discernible trend in the response to hydrogen.

1 | Introduction

Hydrogen is increasingly valued as a clean energy source, sparking renewed interest in its impact on the mechanical properties of various steel grades, including medium-strength, high-strength, and stainless steels. Regarding the effect of hydrogen on the fatigue and fracture behavior of steel, the primary technical issue is associated with hydrogen embrittlement. This phenomenon results in the degradation of the material's mechanical properties (including strength and ductility), leading to premature failures during in-service operations. Recognizing the critical nature of hydrogen embrittlement, this topic has been systematically studied by the international scientific community since the early twentieth century. The physical mechanism of hydrogen embrittlement in steels has been thoroughly explored and systematically discussed in the literature [1–4]. In essence, when exposed to hydrogen—either through gaseous environments or electrochemical processes—additional degradation mechanisms can significantly accelerate fatigue damage. This phenomenon is referred to as hydrogen-assisted fatigue or hydrogen-enhanced fatigue crack growth. Hydrogen atoms diffuse into the metal lattice, preferentially accumulating at regions of high triaxial stress such as crack tips. Once inside the material, hydrogen can reduce cohesive forces between atoms (hydrogen-enhanced decohesion), facilitate dislocation motion (hydrogen-enhanced localized plasticity), or promote phase transformations and embrittlement. These mechanisms lead to reduced fatigue life, increased crack propagation rates, and a lower fatigue threshold. The combined effect of cyclic loading and hydrogen presence can result in premature failure, particularly in high-strength alloys and welded joints where hydrogen susceptibility is elevated.

The enormous body of research work on hydrogen effect on the behavior of steels has been summarized in several review articles (see, for instance, [5–13] for the associated physical mechanisms and [14–19] for static behavior and the corresponding physical mechanisms). However, examination of these articles shows that, over the years, attention has been mainly focused on summarizing and describing qualitatively the interaction between hydrogen and metals, with a particular focus on the underlying mechanisms. In contrast, to date, no studies have attempted to review quantitatively the effect of hydrogen on the fatigue and fracture behavior of steel. This explains why the underlying mechanisms are not addressed in the present investigation.

To address this knowledge gap, it is essential to assess the impact of hydrogen on the fatigue properties of steel through statistical and quantitative methods. This paper reports on an in-depth re-analysis of datasets to investigate the fatigue behavior of conventional steel and stainless steel in the presence of hydrogen. Statistical and quantitative methods (such as linear regression analysis, S-N curve plotting, unified S-N curve construction, and Paris' law regression) were systematically and consistently applied to post-process experimental results taken from the technical literature. In this setting, this review primarily focuses on two main areas: plain material fatigue properties (e.g., endurance limit and slope of the S-N curve) and the fatigue crack growth properties (e.g., threshold value of the stress intensity factor range and crack propagation rate) of steel used in the gas transportation industry such as stainless steels—e.g., 17-4PH (AISI 630), AISI304, AISI316, AISI347—or carbon steels—e.g., SCM435 (AISI4135), API 5L X52 pipeline steel, and Si-Cr steel (AISI 9254). The reanalyses presented in this paper are aimed to serve as a valuable reference for researchers, industrialists, and professionals engaged in hydrogen-related structural engineering issues, enhancing our quantitative understanding of the effects of hydrogen exposure on steel structural integrity. In particular, the ultimate aim of this investigation is not to provide engineers and researchers with definitive reference values for use in design and structural integrity analysis. Instead, the goal is to identify potential trends in the constants associated with S-N and Paris' curves when steel components operate in hydrogen-rich environments.

Finally, it is worth noting that, although alternative models could have been used to post-process the experimental results considered in this review, we deliberately chose to adopt standard approaches during the design of this study. The selected models are widely recognized and utilized not only within the research community but also in industry. While the use of more advanced models to describe fatigue strength and crack growth behavior might have yielded different results, such approaches are not yet universally accepted or included in standard guidelines. This explains the reasoning behind the selection of the models used for data post-processing.

2 | Database

The effect of hydrogen on the fatigue and crack growth behavior of steel was assessed through an analysis of experimental fatigue data, which were post-processed in terms of either S-N curves or crack growth curves. In the following two subsections, the fundamental theoretical concepts used in the analyses discussed below will be briefly reviewed, not only to avoid possible terminological misunderstandings but also to unambiguously explain the meaning of the adopted symbols.

2.1 | Fatigue Strength of Un-Cracked Metals

The S-N curve, also known as the Wöhler (or Basquin) curve, is a graphic representation of the relationship between the applied stress and the number of cycles to failure for a material under specific testing conditions. Figure 1 presents a schematic representation of an S-N curve for steel on a log–log scale. The schematic diagram consists of three distinct regimes, namely, the low-cycle fatigue (LCF) regime, the medium-cycle fatigue (MCF) regime, and the high-cycle fatigue (HCF) regime.

Low-cycle fatigue occurs under high-stress conditions, where the material is typically subjected to plastic deformation leading to a failure within a relatively small number of cycles. For metallic materials, this usually occurs in the range of 1 to 10^3 cycles to failure. The fatigue limit is defined as the material-dependent stress level below which the material under investigation can theoretically withstand an infinite number of cycles to failure. For materials with a fatigue limit, the S-N curve in the high cycle fatigue regime features a horizontal asymptote, with the corresponding stress amplitude (or range) representing the material's fatigue limit [20]. This classic definition predates more modern findings in the giga-cycle fatigue regime [21]. Modern research has revealed that many factors can eliminate the fatigue limit, leading to a different reference strength definition for high-cycle fatigue. Accordingly, when a fatigue limit cannot be identified unambiguously or when the materials under investigation do not exhibit a fatigue limit (such as, for instance, aluminum alloys), a reference strength is estimated at N_A cycles to failure. This usually lies in the range $5 \cdot 10^5 \div 10^7$ cycles to failure [22]. This reference stress is referred to as the "endurance limit." Given the challenges in defining the fatigue limit for different materials, in the present investigation, the endurance limit concept was used, with this high-cycle fatigue reference strength being estimated at $N_A = 2 \times 10^6$ cycles to failure. In this context, it is important to clarify that a material being at its endurance limit does NOT mean it can endure an infinite number

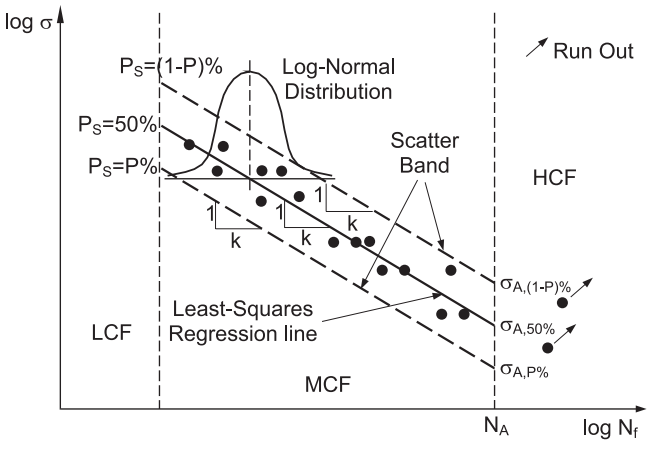

FIGURE 1 | Schematic representation of an S-N curve and its associated scatter band.

of cycles at that stress level. Rather, the endurance limit signifies that the material can survive up to a specific number of cycles—referred to as N_A in this study. However, at the endurance limit stress level, the material may still fail shortly after reaching a number of cycles equal to N_A. These considerations suggest that, in this study, the term "endurance limit" is used to denote a reference strength in the high-cycle fatigue regime and NOT as a conventional "fatigue limit"—i.e., a stress threshold below which the material can endure an infinite number of cycles. From a quantitative review standpoint, one of the key advantages of using the endurance limit is that, when systematically estimated through statistical analysis, it provides a consistent basis for comparing and contrasting results from different experimental trials. Another important implication is that, given the negative inverse slope and the endurance limit at N_A cycles to failure, it is possible to estimate a different reference high-cycle fatigue strength for a different number of cycles to failure if needed. In this study, $N_A = 2 \times 10^6$ cycles to failure was selected as a reference, following recommendations from established standard codes and guidelines for fatigue assessment of welded joints, such as Eurocode 3 and the Recommendations of the International Institute of Welding.

As far as the effect of hydrogen on the fatigue behavior of metals is concerned, this paper focuses on experimental results generated in the MCF regime (i.e., the central region in Figure 1). Data reanalysis involved calculating the corresponding S-N curve and associated scatter band in a log–log domain. S-N curves were derived by fitting a linear function to experimental results, as shown below [20, 23]:

$$Log\, N_f = C_o + C_1 Log\, \sigma \tag{1}$$

where N_f is the number of cycles to failure (i.e., the fatigue lifetime), σ is the stress level (that can be expressed in terms of either range, amplitude or maximum value), and C_o and C_1 are the intercept and inverse slope of the log–log linear function, respectively. These are constants that vary for different materials, load ratios and environmental conditions.

In the present study, the linear regression method (LRM) was applied to fit the mean S-N curve to the experimental fatigue datasets that were collected. The LRM uses the least squares approximation [24, 25] to determine the slope and intercept of the mean curve by minimizing the sum of the square of the differences between the observed dependent variable (fatigue life) and the output of the linear function of the independent variable (stress levels). Constants C_0 and C_1 are estimated from the experimental results as follows [26]:

$$C_1 = \frac{\sum_{i=1}^{n} \left[\log(\sigma_i) - \overline{log\sigma_i}\right]\left[\log(N_i) - \overline{logN_i}\right]}{\sum_{i=1}^{n} \left[\log(\sigma_i) - \overline{log\sigma_i}\right]^2} \tag{2}$$

$$C_0 = \overline{logN_i} - C_1 \overline{log\sigma_i} \tag{3}$$

where n is the sample size and $i = 1, 2 \ldots n$. $\overline{\log \sigma_i}$ is the mean of the log of the stress levels and $\overline{logN_i}$ is the mean of the log of the number of cycles to failure.

Equation (1) can also be rewritten as suggested by Wöhler and Basquin, i.e., by directly using a power law relationship between the applied stress and the number of cycles to failure [27]. Given two reference points having coordinates equal to (σ_A, N_A)—at the endurance limit—and to (σ, N_f), respectively, Wöhler's (or Basquin's) equation takes on the following form:

$$\sigma^k N_f = {\sigma_A}^k N_A = constant \tag{4}$$

where k is the negative inverse slope which is linked with constant C_1 as follows:

$$k = -C_1 \tag{5}$$

Substituting the negative inverse slope in Equation (1), the mean S–N becomes:

$$logN_f = C_o - k \cdot log\sigma_i \tag{6}$$

Accordingly, the endurance limit for the predicted mean curve at the reference number of cycles, N_A, can be expressed as:

$$\sigma_{A,50\%} = \left[\frac{10^{C_0}}{N_A}\right]^{\frac{1}{k}} \tag{7}$$

In Equation (7), subscript 50% is used to explicitly denote that the endurance limit refers to the mean curve, that is to a fatigue curve characterized by a probability of survival, P_S, equal to 50%.

The reference stress level at N_A cycles to failure can be computed for different probabilities of survival via the standard deviation of the population, the endurance limit for $P_s = 50\%$ and another statistical constant, q, depending on the desired survival probability, confidence level, and sample size [28–31].

Thus, the endurance limit at N_A cycles to failure takes on the following values for $P_s = P\%$ and $P_s = (1\text{-}P)\ \%$, respectively:

$$\sigma_{A,P\%} = \sigma_{A,50\%}\left[\frac{N_A}{10^{log(N_A)+qs}}\right]^{\frac{1}{k}} \tag{8}$$

$$\sigma_{A,(1-P)\%} = \sigma_{A,50\%}\left[\frac{N_A}{10^{log(N_A)-qs}}\right]^{\frac{1}{k}} \tag{9}$$

where the variance, s, is calculated as:

$$s^2 = \frac{\sum_{i=1}^{n} \left(LogN_f - LogN_i\right)^2}{n-1} \tag{10}$$

The size of the scatter band associated with the data set being analyzed is defined as the ratio between $\sigma_{A,(1-P)\%}$ and $\sigma_{A,P\%}$. In the present investigation, the level of scattering was quantified as follows [26]:

$$T_\sigma = \frac{\sigma_{A,10\%}}{\sigma_{A,90\%}} \tag{11}$$

where $\sigma_{A,10\%}$ and $\sigma_{A,90\%}$ are the endurance limits calculated for probability of survival P_S equal to 10% and 90%, respectively.

As examples, Figure 2a,b show two S-N curves with the associated scatter bands for two datasets taken from the literature [32, 33] and used in the re-analyses discussed in what follows. In Figure 2, σ_a is the stress amplitude and R is the load ratio, which is defined as the ratio between the minimum, σ_{min}, and maximum, σ_{max}, stress applied in the fatigue cycle.

The analyses summarized in what follows will focus on comparing parameters derived from S-N curves under conditions with and without the presence of hydrogen. Key aspects detailed in Section 3 will include the degree of scatter, T_σ, the endurance limit, $\sigma_{A,50\%}$, for the predicted mean curve at $N_A = 2 \times 10^6$ cycles to failure, and the inverse slope,k.

2.2 | Fatigue Behavior in the Presence of Cracks

The crack propagation behavior of steel in the presence of hydrogen was investigated using crack growth curves. Figure 3a illustrates a schematic diagram of a crack growth curve, also known as Paris' curve, which graphically represents, using a log–log scale, the relationship between the crack growth rate, da/dN, and the stress intensity factor range, ΔK. In this graph, a denotes the crack size, and N represents the number of cycles. Based on the schematic representation of Figure 3a, three distinct different regimes are identifiable as follows.

- Regime I. The stress intensity factor range, ΔK, is below the threshold value of the stress intensity factor range, ΔK_{th} , meaning that the crack growth rate is so low that, from an engineering perspective, no propagation is assumed to occur.
- Regime II. This is the central region of Paris' diagram, where the crack growth rate,da/dN, follows a power-law relationship with ΔK.
- Regime III. In this region, the maximum value of the applied stress intensity factor approaches the material's fracture toughness, K_c, causing the crack growth rate to accelerate rapidly until a sudden, catastrophic failure occurs [35].

This paper focuses specifically on the threshold value of the stress intensify factor range, ΔK_{th}, and the crack growth behavior in Regime II. As far as Regime II is concerned, for a given dataset, the associated curve was generated by fitting the experimental results via the least squares method to determine constants C and m in the following well-known relationship [36]:

$$\frac{da}{dN} = C \cdot \Delta K^m \tag{12}$$

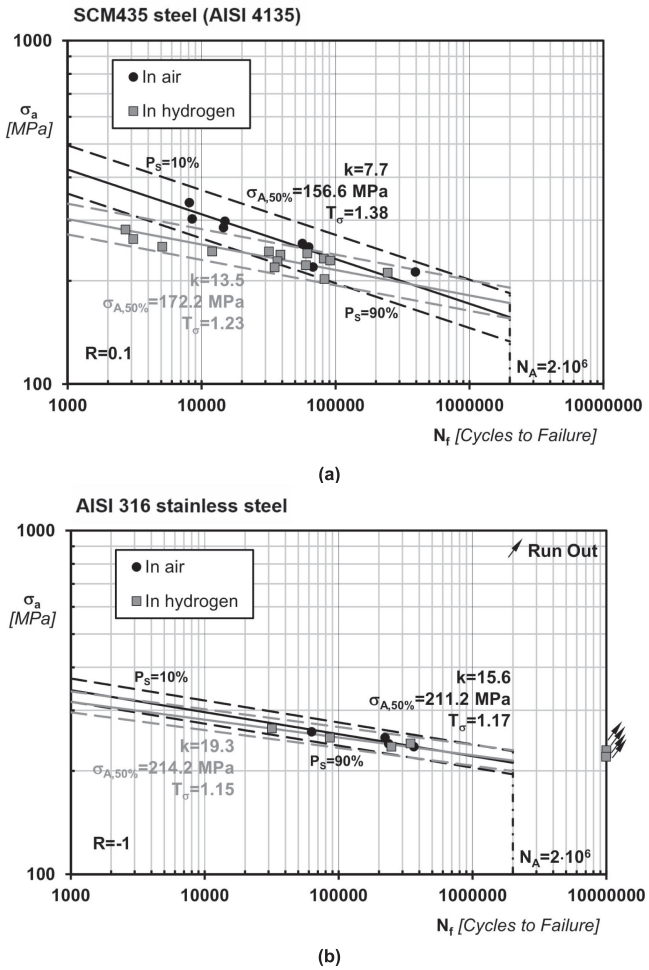

FIGURE 2 | Comparison between the S-N curve in air and in hydrogen for SCM435 steel (AISI 4135) [32] (a) and AISI 316 stainless steel [33] (b).

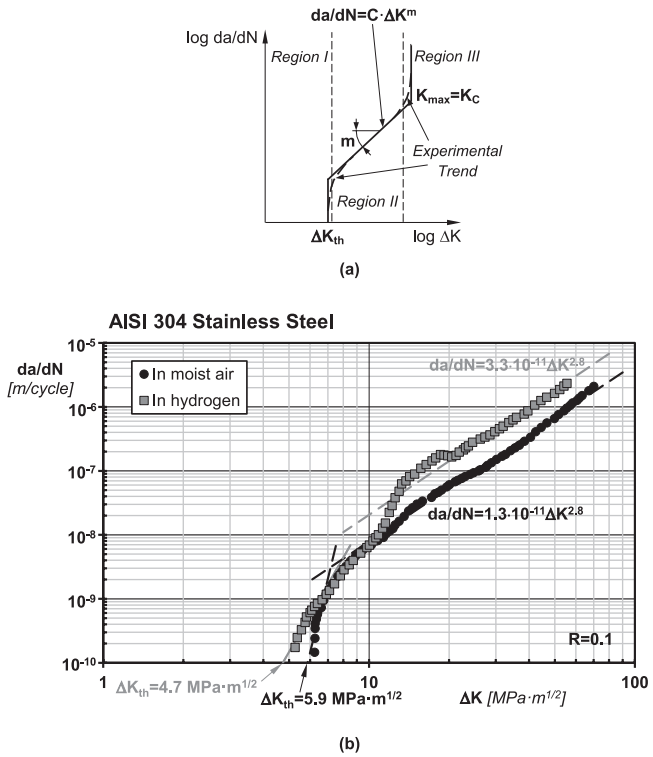

FIGURE 3 | Schematic representation of a fatigue crack propagation curve (a) and comparison between the crack growth curve in inert environment and in hydrogen for AISI 304 stainless steel [34] (b).

From a mathematical standpoint, the linear regression procedure followed is similar to that used for post-processing S-N curves, as previously described.

Since, according to ASTM E647-23a [37], the threshold value of the stress intensity factor range is determined using data characterized by da/dN values in the range of 10^{-9} to 10^{-10} m/cycle, constants C and m in Equation (12) were determined by post-processing only the data points with da/dN values greater than 10^{-8} m/cycle. This strategy allowed us, on the one hand, to effectively estimate the constants C and m by focusing on the region of the Paris diagram where a linear relationship (in a log–log representation) exists between da/dN and ΔK; and, on the other hand, to determine these constants across the various datasets in a consistent manner, enabling meaningful comparisons. Further, to ensure that the data re-analyzed using Equation (12) exhibited a strong linear relationship within Regime II, the correlation coefficient [38] was calculated for each individual dataset. In 94% of the regression analyses, the correlation coefficient exceeded 0.9, with the lowest recorded value being 0.66. These results confirm that the values of the constants C and m reported in Tables 3 and 4 are associated with a strong linear relationship between da/dN and ΔK.

The threshold stress intensity factor range, ΔK_{th}, was estimated using the standard procedure recommended by ASTM E647-23a [37]. According to these guidelines, the operational definition of ΔK_{th} involves identifying the ΔK value corresponding to a finite crack growth rate, da/dN, equal to 10^{-10} m/cycle. More specifically, ΔK_{th} was determined from the best-fit line obtained via linear regression of log (da/dN) versus log (ΔK), using all (da/dN, ΔK) data points collected for each dataset within the crack growth rate range of 10^{-9} to 10^{-10} m/cycle. In line with the ASTM recommendations, datasets containing fewer than five experimental points within this growth rate range were excluded from post-processing for the determination of ΔK_{th}.

The re-analyses discussed below were performed by referring to standard recommendations, as the ASTM standards are the most widely used in industry. Furthermore, it is important to highlight that this widely recognized ASTM approach was adopted also due to the absence of a specific standard addressing the fatigue cracking behavior of metals in hydrogen-rich environments. A key advantage of using the ASTM approach is that ΔK_{th} is estimated by extrapolating the stress intensity factor range value at da/dN equal to 10^{-10} m/cycle. This methodology enables consistent comparison of ΔK_{th} values across different investigations. In summary, we chose the ASTM-recommended approach because, on the one hand, there is no specific standard for hydrogen-related situations, and on the other hand, it provides a standardized method suitable for comparing ΔK_{th} values obtained from different experimental trials.

An illustrative example of crack growth curves generated in the presence and absence of hydrogen is presented in Figure 3b, with data extracted from Ref. [34]. In line with the ASTM standard approach, the reported values of ΔK_{th} were determined by post-processing data points in the range of 10^{-9} to 10^{-10} m/cycle. In contrast, the constants C and m were determined by considering data points with da/dN values greater than 10^{-8} m/cycle. For this specific material and testing conditions, the chart in Figure 3b shows that the presence of hydrogen led to a reduction in the ΔK_{th} value, along with an increase in crack growth rate in Region II.

2.3 | Construction of the Database

The effect of hydrogen on the fatigue and crack propagation behavior of metallic materials was investigated by focusing attention on both conventional and stainless steel. Welded steel was also considered in the analysis of fatigue cracking behavior. The experimental results used to compile this review were selected from relevant technical literature [32–34, 39–115]. The list of all the metallic materials that were considered in the present investigation is reported in Table 1. This table also reports the testing temperature, as well as the hydrogen pressure during both testing and soaking. The material properties seen in Table 1 include Young's modulus, E, yield strength, σ_y, ultimate tensile strength, σ_{UTS}, elongation at failure, E_f, and Vickers hardness, HV.

The fatigue results and fatigue crack growth data were extracted from the original graphs and plots by using open-access software WebPlotDigitizer.

The fatigue data sets considered in the present investigation are listed in Table 2 for un-cracked metals and in Tables 3 and 4 for un-welded and welded cracked metallic materials, respectively.

Table 2 summarizes the fatigue behavior of un-cracked steel in terms of material designation and testing conditions. The experimental fatigue data for each material were re-analyzed using linear regression [30]. The resulting S-N curves are summarized in Table 2 in terms of load ratio, $R = \frac{\sigma_{min}}{\sigma_{max}}$, inverse negative slope, k, endurance limit, $\sigma_{A,50\%}$, at $N_A = 2{\cdot}10^6$ cycles to failure and scatter ratio, T_σ.

Tables 3 and 4 summarize the fatigue cracking behavior of the considered un-welded and welded metallic materials, respectively, in both the absence and presence of hydrogen. For each material, Tables 3 and 4 detail the hydrogen exposure condition, the load ratio, R, testing frequency, F, values of constant C and exponent m in Paris' equation, Equation (12), and the threshold value of the stress intensity factor range, ΔK_{th}, extrapolated at a crack growth rate of 10^{-10} m/cycle as recommended by the ASTM standard procedure [37]. The comparison of the parameters mentioned above, along with a discussion of the results, is presented in Section 4. Finally, it is worth noting that the majority of the fatigue crack growth tests were conducted using C(T) specimens, with efforts made to adhere as closely as possible to ASTM recommendations. This was done while simultaneously managing the additional complexities introduced by the hydrogen charging process. Readers are referred to the original sources for a detailed description of the experimental procedures followed.

3 | Hydrogen Effect on the Fatigue Behavior of Un-Cracked Steel

As far as the fatigue behavior in the presence of hydrogen is concerned, the materials investigated included both conventional steels and stainless steels. The associated S-N curves parameters are summarized in Table 2. The re-analyzed data were divided

TABLE 1 | Mechanical properties of the materials considered in the present investigation [32–34, 39–115].

Material	Type	Ref.	Remarks	Testing temperature [K]	Testing pressure [MPa]	Soaking pressure [MPa]	Mechanical properties				Vickers hardness (HV)
							E [GPa]	σ_y [MPa]	σ_{UTS} [MPa]	E_f [%]	
A286(AISI 660)	Stainless steel	[33]	Precipitation hardened	Room temperature (RT)	0.12		198	600	967	23	393
AISI 316	Stainless steel	[33]	30% Pre-strained	RT	0.12		192	699	746	36	264
		[99]	Heating, rapid cooling	RT		10		242	610	81.8	163
		[101]		RT	100			283	602	63	
		[102]		RT	90			245	551	40	
		[105]	Electric discharge machining	RT		14.7			550		
		[53]		RT	78–115		200	263	586	61	140
	Welded stainless steel	[88]	Plasma arc welding	RT	0.2						
AISI 304	Stainless steel	[33]	30% Pre-strained	RT	0.12		192	657	889	40	311
		[96]	40% pre-strained	RT	0.22			955	1027	26	358
		[101]		RT	100			279	646	60	
		[102]		RT	90			205	520	40	
		[34]	Cold-rolled, annealed	RT				351	617	57.4	
AISI 304	Stainless steel	[40]	Heat-treated at 1100 °C, water quenching	RT	0.7			274	628		
		[53]		RT	78–115		200	258	612	66	155
		[77]	Laser welding and laser surface treatment	RT	0.2			367	720	68	
		[85]		RT	5×10^{-5}-3			259	655	58	
	Welded stainless steel	[87]	Plasma arc welding	RT	0.2						

(Continues)

TABLE 1 | (Continued)

Material	Type	Ref.	Remarks	Testing temperature [K]	Testing pressure [MPa]	Soaking pressure [MPa]	Mechanical properties				Vickers hardness (HV)
							E [GPa]	σ_y [MPa]	σ_{UTS} [MPa]	E_f [%]	
JIS G4052 Grade SCM435H(AISI 4135)	Chromium molybdenum steel	[32]		RT	0.7–90			1061	1091	14	368
		[33]	Quenched and tempered	RT	0.12		206	788	944	21	293
		[93]	Quenched, water-sprayed and tempered	RT	5.5/34			671	824		256
		[95]	Tempering, heating and oil quenching.	RT	0.1				2050		600
		[106]	Surface polished	RT	45			781	958	58	
		[42]	Water-quenching after keeping the temperature at 830 °C for 2 min	RT		63		835–1080	980–1180		330
0.7C-13Cr (AISI 420)	Stainless steel	[92]		RT							675
API 5L X52	Pipeline steel	[97]						410	528	15.8	
		[47]		RT	1.7–48			429	493		200–250
		[56]			1.4–20.7		206	325	526		
		[57]	Tempered at 550 °C, hot rolling	RT		6.3		497	592	15.9	
		[61]		RT	5.5/34			325	526		
JIS G3106 Grade SM490B	Structural steel	[93]	Quenched, water-sprayed and tempered	RT	115			671	824		256
		[60]	Annealed and cold worked	RT	0.1–90			360	540	17	153
		[72]		298–423 K	0.7–90			360	537		
JIS SWOSC-V (AISI 9254)	Silicon-chromium steel	[107]	Austenitized, oil quenching and tempering						1849		
17-4PH (AISI 630)	Stainless steel	[94]	Water quenching, precipitation hardening, air cooling	RT		35/100			1013		

(Continues)

TABLE 1 | (Continued)

Material	Type	Ref.	Remarks	Testing temperature [K]	Testing pressure [MPa]	Soaking pressure [MPa]	Mechanical properties				Vickers hardness (HV)
							E [GPa]	σ_y [MPa]	σ_{UTS} [MPa]	E_f [%]	
JIS G4051 Grade S45C (AISI 1045)	Medium carbon steel	[98]	Annealed, machined	RT							185
UFG16-10 (AISI 321)	Stainless steel	[99]	Heating, rapid cooling	RT		10		585	793	50	295
CG16-10 (AISI 321)	Stainless steel	[99]		RT		10		156	629	66.2	145
AISI 347	Stainless steel	[103]		RT	34.5			720	1378	43	
		[104]	Heat-treated, water quenched	RT				310	658	61	
SCM440 (AISI 4140)	Chrome alloy structure steel	[106]	Surface polished	RT	45			875	1018	54	
		[54]	Tempered at 843 K	RT				917	1036	18	325
		[68]	Heated at 1133 K for 2.5 h and tempered at 733 K for 3 h	RT	9			1232	1365	11.7	437
API 5L X100	High-strength steel	[43]		RT				260	440		
	Welded high-strength steel	[91]	Gas metal arc welding	RT	21		207	705	780		
ASTM A333 steel	Alloy steel	[44]		RT	0.11			355	481	44	136

(Continues)

TABLE 1 | (Continued)

Material	Type	Ref.	Remarks	Testing temperature [K]	Testing pressure [MPa]	Soaking pressure [MPa]	Mechanical properties				Vickers hardness (HV)
							E [GPa]	σ_y [MPa]	σ_{UTS} [MPa]	E_f [%]	
API 5L X80	High strength steel	[45]	TMCP rolling finishing above the Ar3 followed by ACC (water) cooling	RT	5.5/11/20.7			541	596	40	
		[46]	Polished with a 2000 grade SiC paper and then cleaned ultrasonically in acetone	RT	12			523.9	656.39	26.88	
		[41]		RT	6			552	655	24	
		[71]		RT	10			660	724		
		[74]		RT		30	209	507	677	26	
	Welded High strength steel	[89]	Spiral welding	RT	12						
		[90]	Spiral submerged arc welding	RT	0.7–115		205	599.7	566.2	18.8	
API 5L X60	High strength steel	[39]		RT	6.9						
		[45]	TMCP rolling finishing above the Ar3 followed by ACC (water) cooling	RT	5.5/11/20.7			435	486	42	
A106 Gr B pipeline steel (AISI 1020)	Welded carbon steel	[86]	GTAW (gas tungsten arc welding) + SMAW (shield metal arc welding)	RT				380	502		
API 5L X70	High strength steel	[39]		RT	6.9						
		[50]		RT		6.9		485	600		
		[66]	Polished to a fine surface finish	RT	5.5/34			509	609	13	
	Welded High strength steel	[49]		RT	7–21			525	619.1		218.8
API 5L X42	High strength steel	[39]		RT	6.9						
		[56]			6.9		206	366	511		

(Continues)

TABLE 1 | (Continued)

Material	Type	Ref.	Remarks	Testing temperature [K]	Testing pressure [MPa]	Soaking pressure [MPa]	Mechanical properties				Vickers hardness (HV)
							E [GPa]	σ_y [MPa]	σ_{UTS} [MPa]	E_f [%]	
A516 (AISI 1330)	Carbon steel	[39]		RT	6.9						
2-25Cr-1Mo steel (AISI 4140)	Alloy steel	[48]	Heat-treated	RT	0.138			500	610		
		[59]	Austenitized at 925 °C for 90 min, austenitized at 940 °C for 30 min, quenched in water, tempered at 600 °C for 2 h in water, tempered at 650 °C for 2 h	RT		19.5		622	710	22	201
		[81]		RT	0.133			748	819	21	
		[82]	Normalizing for 5.5 h at 954 °C, air cooling, tempered for 8 h at 691 °C, stress relieved for 15 h at 593 °C, 22 h at 649 °C, and 18 h at 691 °C	RT				345	528	29	
SA-542-3 (ASTM A542)	Alloy steel	[48]	Heat-treated	RT	0.138			770	820		
JIS-SNCM439 (AISI 4340)	Conventional steel	[51]	Heat treated, quenching	RT	0.7–80	100			903–933		
		[83]	Annealing, quenching, and tempering	RT	9.9			832	991	10.2	
22-Cr-5-Ni (AISI 2507)	Stainless steel	[52]		RT			190–210	565	827	35	
25-Cr-7-Ni (AISI 2507)	Stainless steel	[52]		RT			190–210	556	814	31	

(Continues)

TABLE 1 | (Continued)

Material	Type	Ref.	Remarks	Testing temperature [K]	Testing pressure [MPa]	Soaking pressure [MPa]	Mechanical properties				Vickers hardness (HV)
							E [GPa]	σ_y [MPa]	σ_{UTS} [MPa]	E_f [%]	
AISI 4130 steel	Conventional steel	[55]	Heat treated	RT	45/70/87.5/100		214	700	830		
		[62]	Quenched and tempered, with a tempered martensitic microstructure	RT			220	715	950		
		[70]	Quenched at 900 °C and tempered at 615 °C, followed by air cooling	RT	92			719	839		
API 5L Grade B	Conventional steel	[56]			1.4/20.7		206	371	539		
S25C (AISI 1025)	Conventional steel	[58]		RT	21			252	464		
S55C (AISI 1055)	Conventional steel	[58]		RT	21			289	615		
SUH660 steel (AISI 660)	Stainless steel	[108]	Solution treated for 1 h at 980 °C, aged for 16 h at 720 °C, and then air cooled	RT		10		664	1065	27.6	
11.4Ni stainless steel (AISI 304)	Stainless steel	[109]		RT	10			234	790	61	
AISI 4140 steel	Conventional steel	[63]		RT	10				1313		393
		[65]	Quenching and tempering, austempering.	RT	0.02			1474	1701	13	
								1528	1720	11.9	
HSLA steel (AISI 4140)	Conventional steel	[64]		RT				650	740		280
AISI 301	Stainless steel	[111]	Cold rolled	293 K				1462	1550		490
Vascomax T-250 (AISI 250)	Conventional steel	[67]	Laser surface annealing (LSA), H900 aging treatment	RT					1720		520
DP1180	Conventional steel	[112]	Cold-rolled	RT				780	1180	8.7	

(Continues)

TABLE 1 | (Continued)

Material	Type	Ref.	Remarks	Testing temperature [K]	Testing pressure [MPa]	Soaking pressure [MPa]	Mechanical properties				Vickers hardness (HV)
							E [GPa]	σ_y [MPa]	σ_{UTS} [MPa]	E_f [%]	
16Mn TWIP steel	Twinning-Induced Plasticity steel	[69]	Gas-phase thermal hydrogen charging at 300 °C, 16 MPa, for 200 h, mechanically ground, polished, and etched	RT	5			334	830	73.8	
25Mn TWIP steel	Twinning-Induced Plasticity steel	[69]	Gas-phase thermal hydrogen charging at 300 °C, 16 MPa, for 200 h, mechanically ground, polished, and etched	RT	5			370	820	57.8	
Ni-based superalloy 718	Nickel-based superalloy	[73]	Mirror-finished by polishing with a 1-μm-diamond suspension	RT	95	100		1100	1350		
		[111]	Precipitation-hardenable, annealed for 1 h at 975 °C and cooled in air. Heat treatment occurs at 720 °C for 8 h and then cooled by 50 °C/h in an oven for 2 h until 620 °C	293 K	0.15–0.2			1100	1375		450
Ti–6Al–4V alloy (AISI B1112)	Titanium alloy	[75]	Mill-annealed	RT	0.245			916	936	18	
SAE52100 (AISI 52100)	Conventional steel	[76]	Oil-quenched from 1113 K, tempered at 643 K, machined to final dimensions after tempering and finished by buffing after polishing with #2000 emery paper.	RT		100		1794	1900		
GB 20 grade steel (AISI 1020)	Conventional steel	[78]	Hot-rolled	RT	0.4			288	422		

(Continues)

TABLE 1 | (Continued)

Material	Type	Ref.	Remarks	Testing temperature [K]	Testing pressure [MPa]	Soaking pressure [MPa]	Mechanical properties				Vickers hardness (HV)
							E [GPa]	σ_y [MPa]	σ_{UTS} [MPa]	E_f [%]	
JIS-SS400 (AISI 1030)	Conventional steel	[79]	Hot-rolled	RT	1/40			314	443	43.3	
Zeron 100 duplex stainless steel	Stainless steel	[80]		RT	0.095			600	700–800		
JIS-SUJ2 (AISI 52100)	Conventional steel	[84]	Tempered at 823 K, quenching					1200	1400	400	
Cr-Ni-Mn austenitic stainless steel (AISI 304)	Stainless steel	[113]	Cast, hot rolled into a 13 mm thick plate, and solution treated	223 K	40			287	663	72	
Cold-drawn eutectoid steel (AISI 1060)	Conventional steel	[114]	Cold drawing and low-temperature annealing at 473 K for 15 min	203 K					2495	40	557
SUS420 (AISI 420)	Stainless steel	[115]	Heat-treated and cold-rolled						1250	7	
Custom 465 (AISI 465)	Conventional steel	[111]	Precipitation hardened (H1000) and kept for 4 h at 538 °C	293 K	0.15–0.2			1510	1593		540

TABLE 2 | Summary of the results from the post-processed S-N curves (endurance limits extrapolated at $N_A = 2{\cdot}10^6$ cycles to failure; subscript H denotes results from tests conducted in the presence of hydrogen).

Ref.	Material	Testing condition	R	F *[Hz]*	S-N curve			*kH/k*	σA,50%-H/ σA, 50%	No. of specimens
					k	σA,50% [MPa]	*Tσ*			
[32]	SCM435 (AISI 4135) Series 1	Test in air	0.1	1	7.7	156.6	1.38	1.76	1.10	8
		Test in gaseous H2	0.1	1	13.5	172.2	1.23			15
[33]	A286 (AISI 660)	Test in air	−1	18.7	2.1	129.8	2.64	2.63	2.00	5
		Test in gaseous H2	−1	18.7	5.4	259.2	1.18			6
[33]	AISI 316 Series 1	Test in air	−1	20	3.2	146.0	2.18	2.24	1.01	3
		Test in gaseous H2	−1	20	7.1	146.8	1.36			4
[33]	AISI 304 Series 1	Test in air	−1	18.7	4.4	162.9	1.11	1.07	1.54	5
		Test in gaseous H2	−1	18.7	4.7	251.5	1.46			6
[33]	SCM435 (AISI 4135) Series 2	Test in air	−1	18.7	3.8	161.7	1.65	2.45	1.09	5
		Test in gaseous H2	−1	18.7	9.4	175.6	1.04			4
[92]	0.7C-13Cr (AISI 420)	Test with un-soaked specimens in air	−1	1–1000	10.2	606.6	2.37	2.20	0.43	5
		Test with hydrogen pre-soaked specimens in air	−1	1–1000	22.4	263.5	3.01			3
[93]	JIS-SM490B	Test in air	−1	1	14.9	239.7	1.13	0.88	0.90	7
		Test in gaseous H2	−1	1	13.1	216.2	1.05			4
[93]	SCM435 (AISI 4135) Series 3	Test in air	−1	1	10.9	323.6	1.22	1.37	1.03	6
		Test in gaseous H2	−1	1	14.8	332.5	1.27			7
		Test in air	−1	1	21.8	274.8	1.41			3
		Test in gaseous H2	−1	1						1
[94]	17-4PH (AISI 630)	Test with uncharged specimens in air	−1	1	3.5	96.8	1.09	1.42	0.96	4
		Test with gaseous hydrogen pre-charged specimens in air	−1	1	5.0	93.1	1.70			4
[95]	SCM435 (AISI 4135) Series 4	Test in air	−1	20	6.9	483.6	1.31	1.50	1.37	6
		Test in gaseous H2	−1	20	10.3	660.4	2.00			4
		Test in gaseous N2	−1	20	19.6	763.8	1.36			3

(Continues)

TABLE 2 | (Continued)

Ref.	Material	Testing condition	R	F *[Hz]*	S-N curve			*kH/k*	σA,50%-H/σA, 50%	No. of specimens
					k	σA,50% [MPa]	*Tσ*			
[96]	AISI 304 Series 2	Test with uncharged specimens in air	−1	20	6.7	197.2	7.04	1.08	0.91	3
		Test with hydrogen cathodically charged specimens in air	−1	20	7.2	180.2	4.21			4
		Test with gaseous hydrogen pre-charged specimens in air	−1	20	6.6	175.8	16.05			3
[97]	API 5L X52	Test with uncharged specimens in air	0.1	10	43.8	249.1	1.02	1.79	1.01	8
		Test with hydrogen electrochemical pre-charged specimens in air	0.1	10	78.5	252.1	1.01			6
[98]	JIS-S45C (AISI 1045)	Test with hydrogen pre-soaked specimens in air	−1	20	17.5	213.7	1.15	1.22	1.04	4
		Test with un-soaked specimens in air	−1	20	14.4	206.4	1.17			3
[99]	UFG16–10 (AISI 321)	Test with uncharged specimens in air	−1	15	7.3	244.6	2.00	5.09	1.39	3
		Test with gaseous hydrogen pre-charged specimens in air	−1	15	37.3	338.7	1.01			3
[99]	CG16–10 (AISI 321)	Test with uncharged specimens in air	−1	15	41.9	205.9	N/A	0.84	0.90	2
		Test with gaseous hydrogen pre-charged specimens in air	−1	15	26.4	186.0	N/A			2
[99]	AISI 316 Series 2	Test with uncharged specimens in air	−1	15	32.0	207.2	1.33	0.84	0.89	4
		Test with gaseous hydrogen pre-charged specimens in air	−1	15	26.8	183.4	1.00			3
[100]	AISI 304 Series 3	Test with un-soaked specimens in air	0.1	0.1–10	5.2	109.6	1.25	1.84	0.94	11
		Test with hydrogen pre-soaked specimens in air	0.1	0.1–10	9.6	102.6	1.13			5
[101]	AISI 304 Series 4	Test in air	−1	1	15.2	218.0	1.09	2.15	1.10	10
		Test in gaseous H2	−1	1	32.7	239.3	1.13			7
[101]	AISI 316 Series 3	Test in air	−1	1	16.4	213.8	1.08	1.49	1.07	9
		Test in gaseous H2	−1	1	24.5	228.6	1.16			7
[102]	AISI 304 Series 5	Test in air	−1	1	12.5	176.8	1.29	1.13	0.95	5
		Test in gaseous H2	−1	1	14.1	167.6	1.28			5
[102]	AISI 316 Series 4	Test in air	−1	1	5.3	92.3	1.08	1.27	1.16	4
		Test in gaseous H2	−1	1	6.8	107.4	1.08			4

(Continues)

TABLE 2 | (Continued)

Ref.	Material	Testing condition	R	F *[Hz]*	S-N curve			*kH/k*	σA,50%-H/σA, 50%	No. of specimens
					k	σA,50% [MPa]	*Tσ*			
[103]	AISI 347 Series 1	Test in gaseous He	0.1	20	24.9	566.0	1.43	1.49	1.07	4
		Test in gaseous H2	0.1	20	37.0	604.8	1.08			4
[104]	AISI 347 Series 2	Test in air	0.1	5	13.1	167.8	1.10	0.42	0.57	6
		Test in H2SO4 solution	0.1	5	5.4	96.0	1.24			7
[105]	AISI 316 Series 5	Test in air	−1	20	15.6	211.2	1.17	1.24	1.01	4
		Test in gaseous H2	−1	20	19.3	214.2	1.15			4
		Test in air	−1	20	27.7	206.1	1.18	0.75	0.96	5
		Test in gaseous H2	−1	20	20.6	197.0	1.25			6
[106]	SCM435 (AISI 4135) Series 5	Test in gaseous H2	−1	1–10	5.3	283.2	2.54	1.59	0.69	4
		Test in air	−1	1–10	3.3	196.5	2.86			8
[106]	SCM440 (AISI 4140)	Test in gaseous H2	−1	1–10	5.5	325.5	1.14	1.81	0.49	5
		Test in air	−1	1–10	3.0	160.1	1.70			4
[107]	Si-Cr steel (AISI 9254)	Test with uncharged specimens in air		83	27.7	587.8	1.05			5
		Test with hydrogen electrochemical pre-charged specimens in air		83	7.8	405.6	1.12	0.28	0.69	4
[40]	AISI 304 Series 6	Test in air	0.1	1	9.1	87.1	1.46	1.54	1.14	6
		Test in gaseous H2	0.1	1	14.0	99.3	1.98			5
[41]	API 5 L X80	Test in gaseous N2	0.1	1	5.1	63.5	1.42	1.39	1.13	12
		Test in gaseous H2	0.1	1	7.1	71.5	1.50			12
[108]	SUH660 steel (AISI 660)	Test with uncharged specimens in air	−1	55	6.4	221.9	1.29	1.08	1.15	6
		Test with gaseous hydrogen pre-charged specimens in air	−1	28	6.9	255.7				2
[109]	11.4Ni SS (AISI 304)	Test in gaseous He	0.1	1	6.6	134.7	1.39	1.33	1.25	6
		Test in gaseous H2	0.1	1	8.8	168.1	1.66			7
[110]	SNCM439 (AISI 4340)	Test with uncharged specimens in air	−1	20	4.9	162.8	1.54	2.88	2.09	5
		Test with gaseous hydrogen pre-charged specimens in air	−1	20	14.1	340.0	1.92			4

(Continues)

TABLE 2 | (Continued)

Ref.	Material	Testing condition	R	F *[Hz]*	S-N curve			*kH/k*	σA,50%-H/ σA, 50%	No. of specimens
					k	σA,50% [MPa]	*Tσ*			
[111]	AISI 301	Test in air	−1	2	4.5	434.9	1.27	0.93	0.97	9
		Test in gaseous H2	−1	2	4.2	422.9	1.31			10
	Custom 465 (AISI 465)	Test in air	−1	2	5.3	447.6	1.62	0.96	1.08	10
		Test in gaseous H2	−1	2	5.1	484.1	1.39			10
	Inconel 718	Test in air	−1	2	4.1	249.2	1.47	1.26	1.26	11
		Test in gaseous H2	-1	2	5.2	313.9	1.31			9
[112]	DP1180	Test with uncharged specimens in air	0.1	1	11.5	335.6	1.28	0.94	1.00	9
		Test with hydrogen electrochemical pre-charged specimens in air	0.1	1	10.9	334.1	1.19			6
[113]	Cr-Ni-Mn austenitic stainless steel (AISI 304)	Test in air	0.1	1	6.5	190.9	1.17	0.76	0.71	7
		Test in gaseous H2	0.1	1	4.9	135.5	1.22			7
[114]	Cold-drawn eutectoid steel (AISI 1060)	Test with uncharged specimens in air	0	30	3.4	490.7		1.83	1.81	3
		Test with hydrogen electrochemical pre-charged specimens in air	0	30	6.1	889.0	1.65			4
[115]	AISI 420	Test with uncharged specimens in air	0.1	30	7.0	160.4	1.22	0.96	0.78	3
		Test with hydrogen electrochemical pre-charged specimens in air	0.1	30	6.7	124.9	2.90			4

TABLE 3 | Summary of the results from the post-processed fatigue crack growth curves generated by testing un-welded steel (threshold value of the stress intensity factor range extrapolated at da/dN = 10^{-10} m/cycle; constant C was determined by measuring ΔK in units of MPa·$m^{1/2}$ and da/dN in units of m/cycle; C_H indicates the hydrogen concentration).

Ref.	Material	Testing conditions	R	F [Hz]	C	m	ΔK_{th} [MPa·$m^{1/2}$]
[39]	API 5L X70	Test in gaseous H_2	0.1	1	$3.25 \cdot 10^{-12}$	4.3	
		Test in gaseous N_2	0.1	1	$1.25 \cdot 10^{-11}$	2.9	
	API 5L X42	Test in gaseous H_2	0.1	1	$3.81 \cdot 10^{-14}$	6.5	
		Test in gaseous N_2	0.1	1	$5.27 \cdot 10^{-13}$	3.9	
	API 5L X60	Test in gaseous H_2	0.1	1	$6.94 \cdot 10^{-12}$	3.8	
		Test in air	0.1	1	$3.06 \cdot 10^{-13}$	4.2	
	A516 (AISI 1330)	Test in gaseous H_2	0.1	1	$5.06 \cdot 10^{-14}$	5.5	
		Test in air	0.1	1	$9.83 \cdot 10^{-13}$	3.7	
	1020 (AISI 1020)	Test in gaseous H_2	0.1	1	$2.93 \cdot 10^{-12}$	4.0	
		Test in air	0.1	1	$1.11 \cdot 10^{-12}$	3.4	
[40]	AISI 304	Test in air	0.1	1	$3.30 \cdot 10^{-12}$	3.28	
		Test in gaseous H2	0.1	1	$1.01 \cdot 10^{-11}$	3.57	
[41]	API 5L X80	Test in gaseous N2	0.1	1	$2.43 \cdot 10^{-7}$	1.42	
		Test in gaseous H2	0.1	1	$3.76 \cdot 10^{-13}$	7.31	
[42]	SCM435 (AISI 4135)	Test with H-uncharged specimens	-1	20	$5.31 \cdot 10^{-12}$	2.6	
		Test with hydrogen cathodic charged specimens	-1	20	$8.62 \cdot 10^{-10}$	1.4	
		Test with H-uncharged specimens	-1	2	$1.07 \cdot 10^{-11}$	2.5	
		Test with hydrogen cathodic charged specimens	-1	2	$5.18 \cdot 10^{-9}$	1.2	
		Test with H-uncharged specimens	-1	0.2	$1.37 \cdot 10^{-11}$	2.5	
		Test with hydrogen cathodic charged specimens	-1	0.2	$2.66 \cdot 10^{-10}$	2.1	
[43]	API 5L X100	Test with specimens cathodic charged in NS4 solution: $C_H = 0.209$ ppm	0	1	$6.30 \cdot 10^{-11}$	4.8	
		Test with specimens cathodic charged in NS4 solution: $C_H = 0.456$ ppm	0	1	$5.48 \cdot 10^{-10}$	4.3	
		Test with specimens cathodic charged in NS4 solution: $C_H = 0.001$ ppm	0	1	$4.23 \cdot 10^{-12}$	5.8	

(Continues)

TABLE 3 | (Continued)

Ref.	Material	Testing conditions	R	F [Hz]	C	m	ΔK_{th} [MPa·m$^{1/2}$]
[43]	API 5L X100	Test with specimens cathodic charged in NS4 solution: $C_H = 0.209$ ppm	0	1	$2.36 \cdot 10^{-11}$	5.2	
		Test with specimens cathodic charged in NS4 solution: $C_H = 0.514$ ppm	0	1	$1.58 \cdot 10^{-12}$	6.2	
		Test with specimens cathodic charged in NS4 solution: $C_H = 1.231$ ppm	0	1	$9.52 \cdot 10^{-12}$	5.7	
[44]	ASTM A333 steel	Test in pure gaseous H_2	0.1	20	$5.86 \cdot 10^{-18}$	8.0	
		Test in gaseous H_2 + 1000 vppm CO	0.1	20	$7.42 \cdot 10^{-18}$	8.0	
		Test in gaseous H_2 + 10,000 vppm CO	0.1	20	$1.19 \cdot 10^{-16}$	6.9	
		Test in gaseous H_2 + 100,000 vppm CO	0.1	20	$7.58 \cdot 10^{-17}$	6.9	
		Test in air	0.1	20	$1.25 \cdot 10^{-13}$	4.4	
[45]	API 5L X80	Test in gaseous H_2	0.5	1	$4.48 \cdot 10^{-14}$	6.2	
		Test in air	0.5	1	$5.09 \cdot 10^{-13}$	4.1	
	API 5L X60	Test in gaseous H_2	0.5	1	$1.78 \cdot 10^{-13}$	5.7	
		Test in air	0.5	1	$1.79 \cdot 10^{-12}$	3.6	
[34]	AISI 304	Test in Argon	0.1	10	$6.08 \cdot 10^{-12}$	3.0	6.32
		Test in moist air	0.1	10	$1.34 \cdot 10^{-11}$	2.8	5.87
		Test in gaseous H_2	0.1	10	$3.33 \cdot 10^{-11}$	2.8	4.74
[46]	API 5L X80	Test in gaseous N_2	0.1	1	$9.13 \cdot 10^{-12}$	2.8	
		Test in gaseous N2 + 5 vol% H_2	0.1	1	$1.04 \cdot 10^{-10}$	2.8	
		Test in gaseous N2 + 10 vol% H_2	0.1	1	$2.84 \cdot 10^{-10}$	2.6	
		Test in gaseous N2 + 20 vol% H_2	0.1	1	$5.85 \cdot 10^{-10}$	2.4	
		Test in gaseous N2 + 50 vol% H_2	0.1	1	$1.20 \cdot 10^{-9}$	2.4	
[47]	API 5L X52	Test in gaseous H_2 + 10vppm O_2	0.5	1	$2.56 \cdot 10^{-13}$	5.0	
		Test in gaseous H_2 + 100vppm O_2	0.5	1	$7.40 \cdot 10^{-14}$	5.3	
		Test in gaseous H_2 + 1000vppm O_2	0.5	1	$5.57 \cdot 10^{-17}$	7.4	

(Continues)

TABLE 3 | (Continued)

Ref.	Material	Testing conditions	R	F [Hz]	C	m	ΔK_{th} [MPa·m$^{1/2}$]
[48]	2-25Cr-1Mo steel (AISI 4140)	Test in 30%RH moist air	0.05	50	$1.12 \cdot 10^{-12}$	3.5	7.03
		Test in gaseous H_2	0.05	50	$5.39 \cdot 10^{-12}$	3.0	4.51
		Test in 30%RH moist air	0.05	2	$5.95 \cdot 10^{-13}$	3.7	
		Test in gaseous H_2	0.05	2	$2.41 \cdot 10^{-16}$	6.6	
		Test in moist air	0.05	50	$7.80 \cdot 10^{-12}$	2.9	
		Test in dry gaseous H_2	0.05	50	$6.98 \cdot 10^{-12}$	2.8	
		Test in air	0.1	5	$7.08 \cdot 10^{-12}$	2.9	
		Test in gaseous H_2	0.1	5	$8.42 \cdot 10^{-13}$	4.0	
		Test in H_2 sulfidic	0.1	5	$3.40 \cdot 10^{-11}$	3.3	
[48]	SA-542-3 (ASTM A542)	Test in moist air	0.05	50	$1.27 \cdot 10^{-12}$	3.5	7.99
		Test in gaseous dry H_2	0.05	50	$2.97 \cdot 10^{-12}$	3.2	5.43
[49]	API 5L X70	Test in air	0.3	0.1	$7.23 \cdot 10^{-12}$	3.1	
		Test in 100% gaseous CH_4	0.3	0.1	$2.11 \cdot 10^{-11}$	2.9	
		Test in 5% gaseous H_2 balance CH_4	0.3	0.1	$1.34 \cdot 10^{-10}$	3.1	
		Test in 1% gaseous H_2 balance CH_4	0.3	0.1	$4.13 \cdot 10^{-11}$	3.3	
		Test in 10% gaseous H_2 balance CH_4	0.3	0.1	$9.61 \cdot 10^{-11}$	3.1	
[50]	API 5L X70	Test in air	0.1	10	$7.03 \cdot 10^{-14}$	4.02	8.67
		Test under hydrogen electrochemical charging conditions	0.1	10	$6.08 \cdot 10^{-13}$	3.50	
[51]	JIS-SNCM439 (AISI 4340)	Test in gaseous N_2	0.5	1	$2.15 \cdot 10^{-11}$	2.02	
		Test in gaseous H_2	0.5	1	$5.76 \cdot 10^{-13}$	4.15	
[52]	22 Cr 5 Ni duplex stainless steel (AISI 2507)	Test in air	0.1	1	$9.59 \cdot 10^{-12}$	2.68	7.32
		Test under hydrogen electrochemical charging conditions	0.1	1	$2.15 \cdot 10^{-11}$	2.65	
	25 Cr 7 Ni super duplex stainless steel (AISI 2507)	Test in air	0.1	1	$3.89 \cdot 10^{-12}$	2.96	
		Test under hydrogen electrochemical charging conditions	0.1	1	$2.40 \cdot 10^{-12}$	3.50	

(Continues)

TABLE 3 | (Continued)

Ref.	Material	Testing conditions	R	F [Hz]	C	m	ΔK_{th} [MPa·m$^{1/2}$]
[53]	AISI 304	Test in air	0.1	1	$1.93 \cdot 10^{-12}$	3.46	
		Test in gaseous H_2	0.1	1	$6.06 \cdot 10^{-12}$	3.92	
	AISI 316	Test in air	0.1	1	$4.26 \cdot 10^{-12}$	3.18	
		Test in gaseous H_2	0.1	1	$1.69 \cdot 10^{-12}$	3.92	
[54]	SCM440H low-alloy steel (AISI 4140)	Test with uncharged specimens in air	0		$7.83 \cdot 10^{-12}$	2.87	
		Test with hydrogen cathodic charged specimens in air	0		$1.02 \cdot 10^{-9}$	2.00	
[55]	AISI 4130 steel	Test in air	0.1	1	$1.21 \cdot 10^{-9}$	1.50	
		Test in 45 MPa gaseous H_2	0.1	1	$2.20 \cdot 10^{-8}$	1.39	
		Test in 70 MPa gaseous H_2	0.1	1	$3.77 \cdot 10^{-8}$	1.33	
		Test in 87.5 MPa gaseous H_2	0.1	1	$4.60 \cdot 10^{-8}$	1.32	
		Test in 100 MPa gaseous H_2	0.1	1	$2.81 \cdot 10^{-8}$	1.50	
[56]	Grade B pipeline steel (AISI 1020)	Test in air	0.1	10	$1.31 \cdot 10^{-13}$	4.30	
		Test in gaseous H_2	0.1	10	$3.05 \cdot 10^{-13}$	5.04	
	API 5L X42	Test in gaseous N_2	0.1	1	$8.21 \cdot 10^{-13}$	3.83	
		Test in gaseous H_2	0.1	1	$6.16 \cdot 10^{-14}$	6.22	
	API 5L X52	Test in air	0.5	1	$1.09 \cdot 10^{-12}$	3.61	
		Test in gaseous H_2	0.5	1	$1.45 \cdot 10^{-14}$	5.90	
[57]	API 5L X52	Test in gaseous N_2	0.1	1	$1.92 \cdot 10^{-11}$	2.69	
		Test in gaseous H_2	0.1	1	$1.24 \cdot 10^{-10}$	2.90	
[58]	S25C carbon steel (AISI 1025)	Test in air	0.1	1	$2.28 \cdot 10^{-12}$	3.37	
		Test in 0.7 MPa gaseous H_2	0.1	1	$1.17 \cdot 10^{-15}$	6.57	
		Test in air	0.1	1	$2.01 \cdot 10^{-12}$	3.41	
		Test in 90 MPa gaseous H_2	0.1	1	$8.61 \cdot 10^{-10}$	2.44	
	S55C carbon steel (AISI 1055)	Test in air	0.1	1	$1.08 \cdot 10^{-12}$	3.64	
		Test in 0.7 MPa gaseous H_2	0.1	1	$7.64 \cdot 10^{-15}$	5.50	
		Test in air	0.1	1	$1.03 \cdot 10^{-12}$	3.66	
		Test in 90 MPa gaseous H_2	0.1	1	$3.24 \cdot 10^{-11}$	3.28	

(Continues)

TABLE 3 | (Continued)

Ref.	Material	Testing conditions	R	F [Hz]	C	m	ΔK_{th} [MPa·m$^{1/2}$]
[59]	2.25Cr-1Mo steels (AISI 4140)	Test with uncharged specimens in air	0.1	1	$8.39 \cdot 10^{-11}$	2.32	
		Test with gaseous hydrogen pre-charged specimens in air	0.1	1	$9.10 \cdot 10^{-8}$	0.69	
[60]	JIS-SM490B	Test in air	0.1	1	$7.34 \cdot 10^{-13}$	3.70	
		Test in gaseous H_2	0.1	1	$5.83 \cdot 10^{-11}$	3.07	
[61]	API 5L X52	Test in air	0.5	0.1	$4.30 \cdot 10^{-13}$	3.91	
		Test in gaseous H_2	0.5	0.1	$1.92 \cdot 10^{-13}$	5.21	
[62]	AISI 4130 steel	Test with uncharged specimens in air	0.1	0.1	$9.55 \cdot 10^{-12}$	2.77	
		Test with hydrogen cathodic charged specimens in air	0.1	0.1	$6.90 \cdot 10^{-7}$	0.61	
[63]	AISI 4140 steel	Test with uncharged specimens in air	0.1	5	$3.71 \cdot 10^{-12}$	3.34	
		Test under 150 h hydrogen electrochemical charging conditions	0.1	5	$1.34 \cdot 10^{-13}$	5.25	
		Test under 200 h hydrogen electrochemical charging conditions	0.1	5	$1.57 \cdot 10^{-12}$	4.39	
		Test under 250 h hydrogen electrochemical charging conditions	0.1	5	$3.12 \cdot 10^{-13}$	4.81	
[64]	HSLA steel (AISI 4140)	Test with uncharged specimens in air	0.1	1	$3.10 \cdot 10^{-12}$	3.42	
		Test with hydrogen cathodic charged specimens in air	0.1	1	$1.04 \cdot 10^{-8}$	1.07	
[65]	AISI 4140 steel AT300	Test in air	0.1	20	$2.03 \cdot 10^{-12}$	3.34	
		Test in gaseous H_2	0.1	20	$1.57 \cdot 10^{-12}$	3.70	
	AISI 4140 steel QT300	Test in air	0.1	20	$4.64 \cdot 10^{-12}$	3.39	
		Test in gaseous H_2	0.1	20	$6.39 \cdot 10^{-13}$	4.75	
[66]	API 5L X70	Test in air	0.1	1	$1.04 \cdot 10^{-12}$	3.62	
		Test in gaseous H_2	0.1	1	$4.31 \cdot 10^{-11}$	3.61	
[67]	Vascomax T-250 (AISI 250)	Test in air	0.1		$1.45 \cdot 10^{-10}$	2.19	
		Test in gaseous H_2	0.1		$8.66 \cdot 10^{-10}$	1.99	
[68]	JIS SCM440 steel (AISI 4140)	Test in air	0.1	5	$1.79 \cdot 10^{-11}$	2.73	4.33
		Test in gaseous H_2	0.1	5	$8.24 \cdot 10^{-19}$	10.38	4.46

(Continues)

TABLE 3 | (Continued)

Ref.	Material	Testing conditions	R	F [Hz]	C	m	ΔK_{th} [MPa·m$^{1/2}$]
[69]	16Mn TWIP steel	Test in gaseous N_2	0.1	1	$1.70 \cdot 10^{-12}$	3.37	
		Test in gaseous H_2	0.1	1	$2.00 \cdot 10^{-11}$	2.95	
	25Mn TWIP steels	Test in gaseous N_2	0.1	1	$3.10 \cdot 10^{-12}$	3.25	
		Test in gaseous H_2	0.1	1	$2.00 \cdot 10^{-11}$	2.91	
[70]	AISI 4130 steel	Test in air	0.1	1	$1.25 \cdot 10^{-12}$	3.38	
		Test in gaseous H_2	0.1	1	$7.90 \cdot 10^{-12}$	4.04	
[71]	API 5L X80	Test in air	0.1	1	$4.23 \cdot 10^{-10}$	1.72	
		Test in gaseous H_2	0.1	1	$4.24 \cdot 10^{-12}$	2.06	
[72]	JIS-SM490B	Test in air	0.1	1	$3.32 \cdot 10^{-13}$	3.92	
		Test in gaseous H_2	0.1	1	$6.89 \cdot 10^{-12}$	4.01	
[73]	Ni-based superalloy 718	Test in air	0.1	1	$4.83 \cdot 10^{-12}$	2.89	
		Test in gaseous H_2	0.1	1	$3.09 \cdot 10^{-11}$	2.78	
[74]	API 5L X80	Test in air	0.1	10	$3.51 \cdot 10^{-12}$	3.20	
		Test in gaseous H_2	0.1	10	$1.94 \cdot 10^{-12}$	4.39	
[75]	Ti–6Al–4V alloy (AISI B1112)	Test in air	0.1	5	$3.62 \cdot 10^{-11}$	3.03	
		Test in gaseous H_2	0.1	5	$2.55 \cdot 10^{-11}$	3.06	
[76]	SAE52100 (AISI 52100)	Test with uncharged specimens in air	0.1	20	$2.36 \cdot 10^{-12}$	3.89	
		Test with gaseous hydrogen pre-charged specimens in air	0.1	20	$1.15 \cdot 10^{-11}$	4.37	
[77]	AISI 304	Test in air	0.1	20	$1.16 \cdot 10^{-14}$	4.82	
		Test in gaseous H_2	0.1	20	$1.09 \cdot 10^{-12}$	3.94	
	AISI 304	Test in air	0.1	20	$6.10 \cdot 10^{-14}$	4.26	
		Test in gaseous H_2	0.1	20	$3.67 \cdot 10^{-12}$	3.47	
[78]	GB 20 grade steel (AISI 1020)	Test in air	0.1	1	$3.50 \cdot 10^{-14}$	4.47	
		Test in gaseous H_2	0.1	1	$5.97 \cdot 10^{-14}$	4.42	
[79]	JIS-SS400 (AISI 1030)	Test in air	0.1	5	$9.08 \cdot 10^{-12}$	2.99	
		Test in gaseous H_2	0.1	5	$4.21 \cdot 10^{-11}$	3.29	

(Continues)

TABLE 3 | (Continued)

Ref.	Material	Testing conditions	R	F [Hz]	C	m	ΔK_{th} [MPa·m$^{1/2}$]
[80]	Zeron 100 duplex stainless steel	Test in air	0.1	5	$5.28 \cdot 10^{-13}$	3.86	
		Test in gaseous H_2	0.1	5	$6.89 \cdot 10^{-12}$	3.54	
[81]	2¼ Cr-1 Mo (AISI 4140)	Test in vacuum	0.1	5	$5.37 \cdot 10^{-13}$	3.45	
		Test in gaseous H_2	0.1	5	$7.28 \cdot 10^{-13}$	3.96	
[82]	2¼ Cr-1 Mo (AISI 4140)	Test in air	0.05	50	$3.37 \cdot 10^{-14}$	4.55	8.68
		Test in gaseous H_2	0.05	50	$5.70 \cdot 10^{-13}$	3.64	7.32
[83]	SNCM439 steel (AISI 4340)	Test in argon	0.1	5	$1.70 \cdot 10^{-14}$	5.06	
		Test in gaseous H_2	0.1	5	$1.28 \cdot 10^{-13}$	6.34	
[84]	JIS-SUJ2 (AISI 52100)	Test with uncharged specimens in air	-1	1	$1.24 \cdot 10^{-10}$	1.85	
		Test with gaseous hydrogen pre-charged specimens in air	-1	1	$6.98 \cdot 10^{-10}$	1.55	
[85]	AISI 304	Test in air	0.1	1	$1.68 \cdot 10^{-14}$	4.99	
		Test in 3 MPa gaseous H_2	0.1	0.1	$6.16 \cdot 10^{-11}$	3.56	
		Test in 45 MPa gaseous H_2	0.1	0.1	$1.41 \cdot 10^{-11}$	4.09	
		Test in 5 kPa gaseous H_2	0.1	0.1	$1.67 \cdot 10^{-12}$	4.36	
		Test in 50 Pa gaseous H_2	0.1	0.1	$3.54 \cdot 10^{-12}$	3.80	
		Test in 70 MPa gaseous H_2	0.1	0.1	$2.61 \cdot 10^{-12}$	4.63	

TABLE 4 | Summary of the results from the post-processed fatigue crack growth curves generated by testing welded steel (threshold value of the stress intensity factor range extrapolated at da/dN = 10^{-10} m/cycle; constant C was determined by measuring ΔK in units of MPa·$m^{1/2}$ and da/dN in units of m/cycle).

Ref.	Material	Environmental condition	R	F [Hz]	C	m
[49]	API 5L X70 girth welds	100% gaseous CH_4	0.3	0.1	$1.95 \cdot 10^{-14}$	4.5
		1% gaseous H_2 balance CH_4	0.3	0.1	$2.51 \cdot 10^{-15}$	5.5
		10% gaseous H_2 balance CH_4	0.3	0.1	$5.37 \cdot 10^{-16}$	6.1
		5% gaseous H_2 balance CH_4	0.3	0.1	$4.64 \cdot 10^{-12}$	3.9
	API 5L X70 longitudinal seam welds	100% gaseous CH_4	0.3	0.1	$1.64 \cdot 10^{-11}$	2.7
		1% gaseous H_2 balance CH_4	0.3	0.1	$2.99 \cdot 10^{-14}$	4.8
		5% gaseous H_2 balance CH_4	0.3	0.1	$1.93 \cdot 10^{-15}$	5.7
		10% gaseous H_2 balance CH_4	0.3	0.1	$3.56 \cdot 10^{-12}$	3.8
	API 5L X70 girth weld HAZ	100% gaseous CH_4	0.3	0.1	$2.66 \cdot 10^{-12}$	3.1
		5% gaseous H_2 balance CH_4	0.3	0.1	$1.01 \cdot 10^{-11}$	3.5
		1% gaseous H_2 balance CH_4	0.3	0.1	$1.56 \cdot 10^{-12}$	4.0
		10% gaseous H_2 balance CH_4	0.3	0.1	$1.86 \cdot 10^{-12}$	3.9
	API 5L X70 longitudinal seam welds HAZ	100% gaseous CH_4	0.3	0.1	$3.37 \cdot 10^{-12}$	3.3
		5% gaseous H_2 balance CH_4	0.3	0.1	$8.09 \cdot 10^{-16}$	6.1
		1% gaseous H_2 balance CH_4	0.3	0.1	$3.89 \cdot 10^{-12}$	3.2
		10% gaseous H_2 balance CH_4	0.3	0.1	$4.32 \cdot 10^{-13}$	4.7
[86]	A106 Gr B steel pipe (AISI 1020)	Test in air	0.1	1	$1.29 \cdot 10^{-12}$	3.8
		Test in gaseous NaCl	0.1	1	$1.96 \cdot 10^{-10}$	2.5
		Test in mixed gaseous NaCl and H_2S	0.1	1	$2.10 \cdot 10^{-9}$	2.3
[87]	AISI 304 stainless steel welds	Test in air	0.1	20	$1.35 \cdot 10^{-14}$	4.5
		Test in gaseous H_2	0.1	20	$4.18 \cdot 10^{-12}$	3.1
[88]	AISI 316 stainless steel welds	Test in air	0.1	20	$6.94 \cdot 10^{-14}$	4.2
		Test in gaseous H_2	0.1	20	$6.43 \cdot 10^{-12}$	3.1
[89]	API 5L X80 pipeline steel welds	Test in air	0.1	20	$1.46 \cdot 10^{-11}$	2.7
		Test in gaseous H_2	0.1	20	$1.22 \cdot 10^{-9}$	2.1
[90]	API 5L X80 pipeline steel welds	Test in gaseous N_2	0.1	1	$1.07 \cdot 10^{-12}$	3.7
		Test in gaseous H_2	0.1	1	$1.79 \cdot 10^{-10}$	3.0
[91]	API 5L X100 pipeline welds	Test in air	0.5	1	$3.15 \cdot 10^{-12}$	3.2
		Test in gaseous H_2	0.5	1	$1.87 \cdot 10^{-26}$	17.4

into four groups by steel type (i.e., conventional and stainless steel) and load ratio (i.e., $R = 0.1$ and $R = -1$).

Given these four groups of data, a comparative analysis was conducted to compare behaviors in hydrogen and inert environments, focusing on fatigue quantities k and $\sigma_{A,50\%}$. In the ratios used for the reanalyses as reported in Table 2 and Figure 4, the subscript "H" indicates the presence of hydrogen.

Figure 4a,b depict the correlation between endurance limit, $\sigma_{A,50\%}$, negative inverse slope, k, and ultimate tensile strength, σ_{UTS}, for conventional and stainless steels subjected to load ratios of −1 and 0.1. The σ_{UTS} values used in these figures were obtained from tests conducted in the absence of hydrogen.

Figure 4a details the effect of hydrogen on the inverse slope, k, of the S-N curve, where the ratio of k for hydrogen-treated to hydrogen-untreated materials is plotted against σ_{UTS}. Each data point represents the ratio of the k-value in the presence of hydrogen to the k-value in the absence of hydrogen for one of the selected materials. As shown, hydrogen generally increases k, resulting in a flattening of the S-N curve. This is

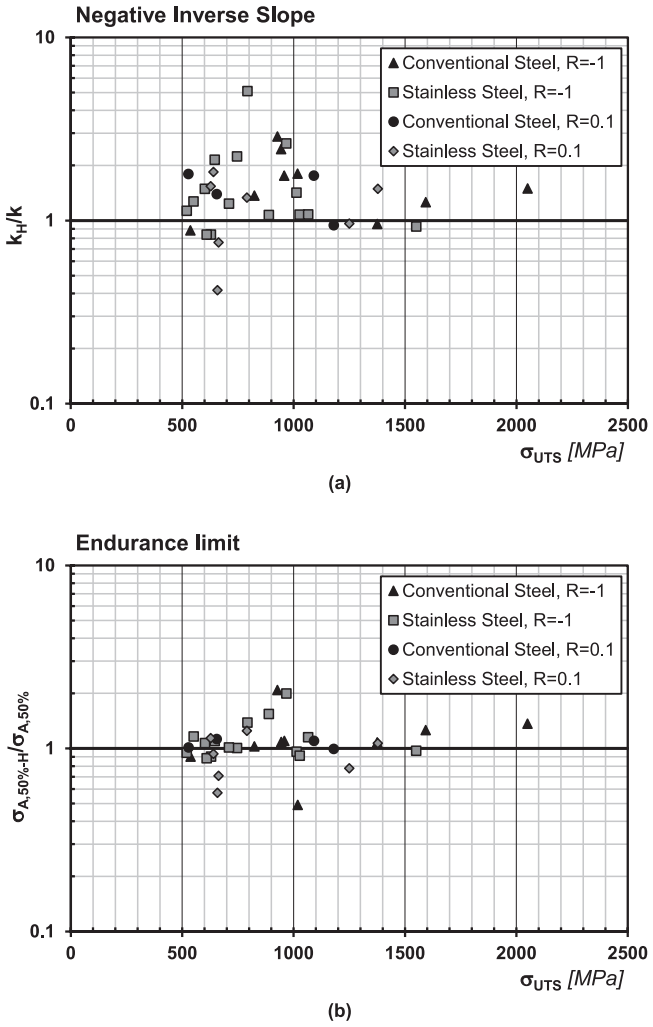

FIGURE 4 | Effect of hydrogen on the negative inverse slope (a) and on the endurance limit (b).

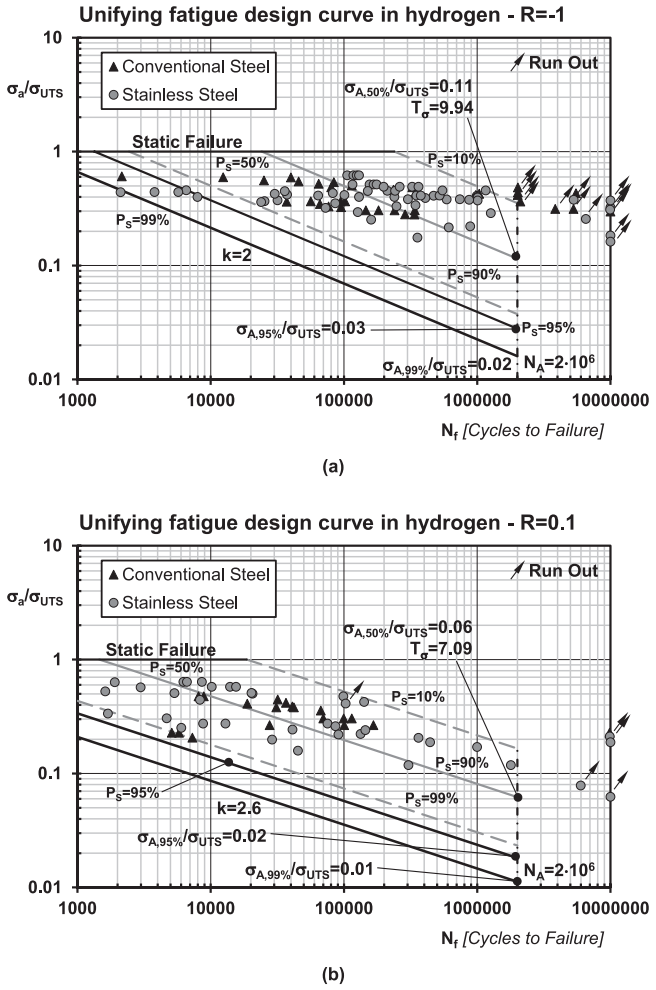

FIGURE 5 | Unifying S-N design curves under a load ratio equal to −1 (a) and to 0.1 (b).

evident from the majority of data points being above a ratio of 1 in Figure 4a.

Figure 4b illustrates the relationship between endurance limit in the presence, $\sigma_{A,50\%-H}$, and in the absence, $\sigma_{A,50\%}$, of hydrogen for both conventional and stainless steels under a stress ratio of −1 as well as of 0.1. As far as conventional steels are concerned, the concentration of the $\sigma_{A,50\%-H}$ to $\sigma_{A,50\%}$ ratios around 1 indicates that hydrogen has a negligible effect on the endurance limit, regardless of the R value. Conversely, for stainless steels, the increased negative slope of the fatigue curves observed in a hydrogen environment results in a modest increase in endurance limit values. Consequently, the $\sigma_{A,50\%-H}$ to $\sigma_{A,50\%}$ ratios are slightly above unity.

It is important to reiterate that all the analyses discussed above are based on the endurance limit estimated at $N_A = 2 \times 10^6$ cycles to failure. The first key consideration is that, as it is not a fatigue limit, fatigue cracks can still initiate at stress levels lower than $\sigma_{A,50\%}$ and $\sigma_{A,50\%-H}$. Furthermore, altering the number of cycles to failure used to define N_A would inevitably affect slightly the trend observed in Figure 4b. However, leveraging Equation (4), the results summarized in Figure 4b can be readily recalculated for different N_A values.

By focusing attention on Figure 2, the fatigue behavior in the presence of hydrogen is further illustrated by comparing the S-N curves and scatter bands for hydrogen-treated and untreated conditions for SCM435 steel (AISI 4135) [32] and AISI316 stainless steel [33]. Quantitative analysis reveals that while the endurance limits remain largely unaffected at 2×10^6 cycles to failure, the S-N curves exhibit significant flattening, indicating reduced fatigue life in the medium-cycle fatigue regime for hydrogen-exposed steels. This suggests a shorter fatigue life in the medium-cycle fatigue regime for hydrogen-treated steels compared to untreated steels at the same stress amplitude.

Based upon this experimental evidence, the subsequent step in the reasoning was to attempt to determine a unified S-N curve that can assess the impact of hydrogen, particularly within the MCF regime. This approach aimed to standardize fatigue analysis under hydrogen exposure by normalizing results via the σ_a to σ_{UTS} ratio, where σ_a represents the applied stress amplitude and σ_{UTS} denotes the material's ultimate tensile strength in the absence of hydrogen. The results of this normalisation process for a load ratio, R, of −1 as well as of 0.1 are summarized in the S-N log–log charts of Figure 5a,b, respectively. The diagram of Figure 5a demonstrates that fatigue life in the MCF regime

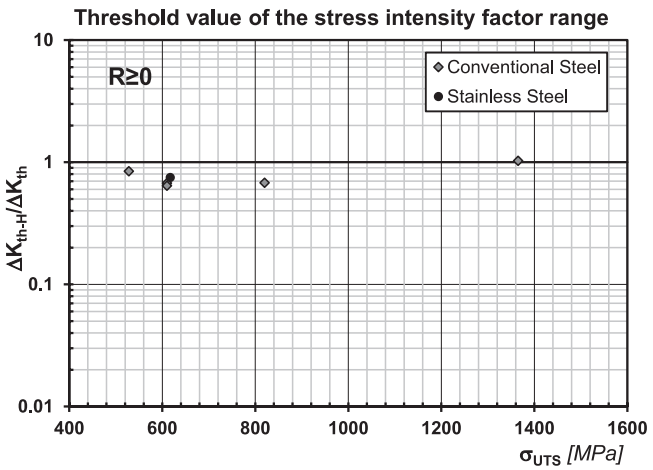

FIGURE 6 | Effect of hydrogen on the threshold value of the stress intensity factor range, ΔK_{th}.

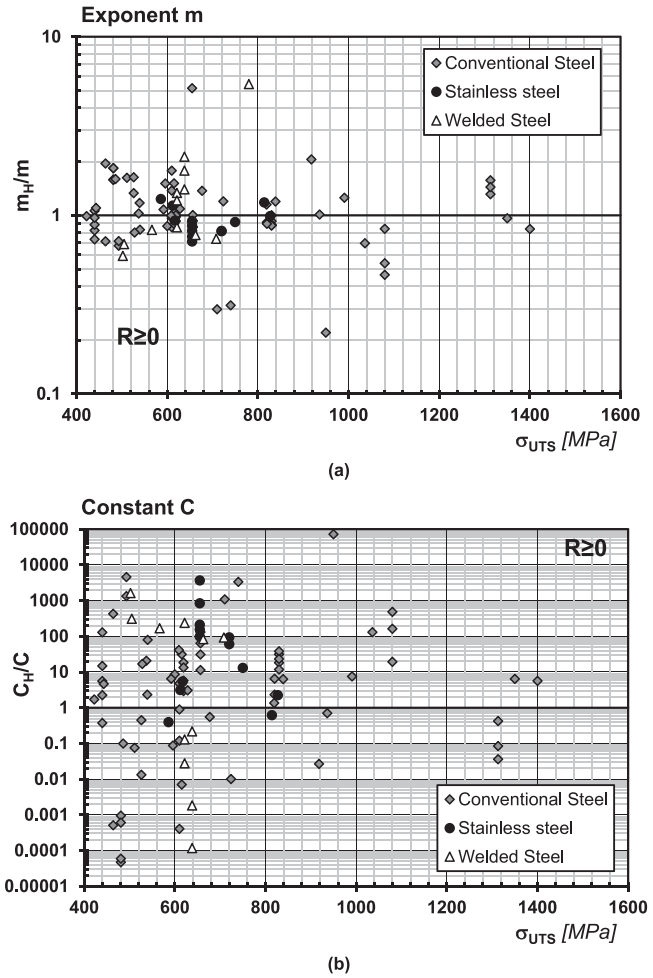

FIGURE 7 | Effect of hydrogen on constants m (a) and C (b) in Paris' crack growth equation. [Colour figure can be viewed at wileyonlinelibrary.com]

under $R = -1$ can be estimated using a fatigue curve with a negative inverse slope, k, of 2 and an endurance limit to ultimate tensile strength ratio of 0.03 for a probability of survival, P_S, of 95% and 0.02 for P_S of 99%. Similarly, The S-N curve in Figure 5b indicates that fatigue life under $R = 0.1$ can be predicted using a fatigue curve with a negative inverse slope, k, of 2.6. For a 95% probability of survival, the endurance limit to ultimate tensile strength ratio is 0.02, whereas for $P_S = 99\%$, the ratio reduces to 0.01. In conclusion, while the two S-N curves reported in Figure 5 provide a safe basis for estimating fatigue life, they are characterized by an excessive level of conservatism. This highlights the need for bespoke experimental investigations as the only effective way to significantly reduce this high degree of conservatism.

4 | Effect of Hydrogen on Fatigue Crack Propagation in Steel

Tables 3 and 4 summarize the post-processed literature data for un-welded and welded steel, respectively. These tables present values of ΔK_{th}, C, and m for different materials with and without hydrogen. Unfortunately, due to the stringent conditions required to determine ΔK_{th} in accordance with ASTM recommendations [37], it was only possible to determine the threshold value of the stress intensity factor range for a limited number of materials.

The results reported in Table 3 and 4 indicate that hydrogen significantly influences fatigue crack growth behavior in metallic materials, but clear trends or patterns are difficult to identify. These tables clearly demonstrate that the effect of hydrogen on fatigue cracking is influenced by the material's morphology and properties, load frequency, and, seemingly, the hydrogen charging technique as well [116]. Therefore, for practical applications, if hydrogen's impact must be evaluated through experiments, it is important to avoid hydrogen charging techniques that are excessively damaging compared to in-service conditions.

To further clarify the above crucial aspects in a quantitative way, the effects of hydrogen on crack propagation were evaluated for stainless steel, carbon steel, and welded steel, with a particular focus on the threshold stress intensity factor, ΔK_{th}, as well as on exponent m and constant C in Paris' equation, Equation (12). The determined values for these parameters are summarized in Tables 3 and 4. The results of the post-processing work are presented in Figures 6 and 7, where the σ_{UTS} represents the values obtained from tests performed in the absence of hydrogen.

Figure 6 presents the ratio of the threshold stress intensity factor range for hydrogen-treated materials, ΔK_{th-H}, to untreated materials, ΔK_{th}, plotted against the ultimate tensile strength, σ_{UTS}. Each data point corresponds to a specific dataset for conventional steel or stainless steel. The horizontal baseline at a ratio of 1 indicates no change in the threshold value of the stress intensity factor range due to the presence of hydrogen. The diagram in Figure 6 confirms that, regardless of material type or σ_{UTS} value, the limited data points all fall below the reference line, indicating that hydrogen generally has a detrimental effect on the threshold stress intensity factor range. However, while the detrimental effect is clear, no consistent trend in terms of reduction magnitude emerges. The lack of a clear trend may also be attributed to the threshold value of the stress intensity factor range in Figure 6 being determined through extrapolation according to the ASTM E647-23a guidelines [37], rather than being experimentally determined.

Figure 7a,b present an analysis for the constant C and exponent m (against σ_{UTS}) in Paris' equation for conventional steel, stainless steel, and welded steel. Constant C is a material-specific parameter that determines the magnitude of the crack growth rate for a given ΔK value. A higher C value indicates a material more prone to faster crack propagation under identical loading conditions, reflecting its inherently lower resistance to fatigue. m represents the slope of the curve on a log–log plot of da/dN vs. ΔK. It quantifies the material's sensitivity to variations in the stress intensity factor range. A steeper slope, m, suggests that small changes in ΔK, result in significant variations in crack growth rate, indicating that the material is highly sensitive to fatigue loading conditions.

In the charts reported in Figure 7a,b, the subscript H denotes constants determined by testing hydrogen-treated specimens. Data points exhibit significant scatter, with values ranging both above and below 1 regardless of material type or σ_{UTS} value. This indicates that there is no clear general trend in how hydrogen affects the crack growth exponent m and constant C: for the exponent m, 47% of the data points are above the baseline, while 53% fall below 1. In contrast, for constant C, 66% of the data points are above the baseline, with 34% of the remaining points below 1.

5 | Conclusions

This review presents a comprehensive quantitative analysis of hydrogen's effects on the fatigue strength and fatigue crack propagation behavior of metallic materials. By systematically re-examining a large dataset of experimental results collected from the literature, we provide a unified framework to summarize how hydrogen influences the structural integrity of metals. Regarding the conclusions reported below, it is crucial to reiterate that the fatigue behavior of uncracked metals in the high-cycle fatigue regime was assessed in terms of the endurance limit estimated at $N_A = 2 \times 10^6$ cycles to failure, rather than the fatigue limit. This distinction implies that when the stress level is set equal to the endurance limit, the material is expected to survive at least up to 2×10^6 cycles, but not an infinite number of cycles. For cracked materials, the threshold value of the stress intensity factor range, ΔK_{th}, was extrapolated at a crack growth rate, da/dn, equal to 10^{-10} m/cycle, following the ASTM standard approach [37]. It is worth noting that this approach is not specifically tailored for hydrogen-soaked metals. The use of the endurance limit and ΔK_{th} values determined according to the ASTM methodology [37] enabled a consistent and systematic comparison of datasets obtained from various experimental campaigns.

Key findings from this analysis can be summarized as follows.

- Overall, hydrogen has a negligible effect on the endurance limit of steel estimated at $N_A = 2 \times 10^6$ cycles to failure, regardless of material type or load ratio.
- Hydrogen generally increases the inverse slope of the S-N curve, flattening it, regardless of material type or load ratio. As a result, for a given stress level, a hydrogen environment reduces fatigue life compared to an inert environment.
- In the absence of specific experimental results, the effect of hydrogen on the fatigue behavior of metallic materials can be assessed using the unifying fatigue curves shown in Figure 5.
- Hydrogen reduces the threshold value of the stress intensity factor range of carbon steels, stainless steels, and steel weldments.
- A systematic evaluation of Paris' constant C and exponent m across all material types revealed significant scatter, indicating no clear trend in their response to hydrogen. However, the presence of hydrogen generally tends to cause an increase in exponent m for conventional steel and a decrease in exponent m for welded steel. Further, the presence of hydrogen tends, on average, to increase the value of constant C.
- The mechanistic phenomena occurring in metallic materials subjected to fatigue loading and exposed to hydrogen are inherently complex, with multiple degradation physical processes acting simultaneously. The specific characteristics of these mechanisms can result in varying degrees of damage. This complexity explains why, in experimental setups, the influence of hydrogen on the fatigue and fracture behavior of metallic materials is significantly affected by the hydrogen charging method employed. Consequently, the experimental approach must replicate, as closely as possible, the conditions experienced during in-service operation.

Nomenclature

a	crack length
da/dn	fatigue crack growth rate
k	inverse slope of the S-N curve
m	Paris' law exponent
C	Paris' law constant
E	Young's modulus
E_f	elongation at failure
F	testing load frequency
HV	Vickers hardness
N	number of cycles
N_f	number of cycles to failure
N_A	reference number of cycles to failure
P_s	probability of survival
R	load ratio (R=$\sigma_{min}/\sigma_{max}$)
T_σ	scatter ratio
ΔK	range of stress intensity factor
ΔK_{th}	threshold value of the stress intensity factor range
σ_a	stress amplitude
σ_y	yield stress
σ_A	endurance limit amplitude
$\sigma_{A,50\%}$	endurance limit amplitude for a probability of survival of 50%
σ_{UTS}	ultimate tensile strength

Author Contributions

H. Wang: data curation; formal analysis; visualization; writing – original draft. **N. O. Larrosa:** supervision; methodology; writing – review and editing. **D. Engelberg:** supervision; methodology; writing – review and editing. **R. Best:** funding acquisition; supervision; methodology; writing – review and editing. **L. Susmel:** funding acquisition; project administration; supervision; conceptualization; methodology; writing – review and editing.

Acknowledgments

National Gas and EPSRC (grant number: EP/W524360/1) are acknowledged for supporting the present research investigation.

Data Availability Statement

The data that support the findings of this study are available from the corresponding author upon reasonable request.

References

1. S. P. Lynch, "2 - Hydrogen Embrittlement (HE) Phenomena and Mechanisms," in *Stress Corrosion Cracking*, eds. V. S. Raja and T. Shoji (Woodhead Publishing, 2011): 90–130.

2. Q. Li, H. Ghadiani, V. Jalilvand, T. Alam, Z. Farhat, and M. A. Islam, "Hydrogen Impact: A Review on Diffusibility, Embrittlement Mechanisms, and Characterization," *Materials.* 17 (2024): 17.

3. V. S. Raja and T. Shoji, *Stress Corrosion Cracking: Theory and Practice* (Woodhead Publishing Ltd, 2011).

4. M. R. Louthan, "Hydrogen Embrittlement of Metals: A Primer for the Failure Analyst," *Journal of Failure Analysis and Prevention*. 8 (2008): 289–307.

5. Y.H. Zhang. *OMAE2010–20622 Review of the Effect of Hydrogen Gas on Fatigue Performance of Steels*, vol. 49149 (International Conference on Offshore Mechanics and Arctic Engineering, 2010): 109–116.

6. A. Pradhan, M. Vishwakarma, and S. K. Dwivedi, "A Review: The Impact of Hydrogen Embrittlement on the Fatigue Strength of High Strength Steel," in *Materials Today: Proceedings*, vol. 26 (Elsevier Ltd, 2019): 3015–3019.

7. N. E. Nanninga, A. J. Slifka, Y. Levy, and C. L. White, "A Review of Fatigue Crack Growth for Pipeline Steels Exposed to Hydrogen," *Journal of Research of the National Institute of Standards and Technology* 115 (2010): 437–452.

8. A. Behvar, M. Haghshenas, and M. B. Djukic, "Hydrogen Embrittlement and Hydrogen-Induced Crack Initiation in Additively Manufactured Metals: A Critical Review on Mechanical and Cyclic Loading," *International Journal of Hydrogen Energy* 58 (2024): 1214–1239.

9. M. Röthig, J. Hoschke, C. Tapia, J. Venezuela, and A. Atrens, "A Review of Gas Phase Inhibition of Gaseous Hydrogen Embrittlement in Pipeline Steels," *International Journal of Hydrogen Energy* 60 (2024): 1239–1265.

10. S. Yang, A. M. P. De Jesus, D. Meng, et al., "Very High-Cycle Fatigue Behavior of Steel in Hydrogen Environment: State of the Art Review and Challenges," *Engineering Failure Analysis* 166 (2024): 166.

11. N. I. I. Mansor, S. Abdullah, A. K. Ariffin, and J. Syarif, "A Review of the Fatigue Failure Mechanism of Metallic Materials Under a Corroded Environment," *Engineering Failure Analysis* 42 (2014): 353–365.

12. A. Behvar and M. Haghshenas, "A Critical Review on Very High Cycle Corrosion Fatigue: Mechanisms, Methods, Materials, and Models," *Journal of Space Safety Engineering.* 10 (2023): 284–323.

13. A. Negi, M. Elkhodbia, I. Barsoum, and A. AlFantazi, "Coupled Analysis of Hydrogen Diffusion, Deformation, and Fracture: A Review," *International Journal of Hydrogen Energy* 82 (2024): 281–310.

14. Y.-S. Chen, C. Huang, P.-Y. Liu, et al., "Hydrogen Trapping and Embrittlement in Metals – A Review," *International Journal of Hydrogen Energy* (2024), https://doi.org/10.1016/j.ijhydene.2024.04.076.

15. W. Li, R. Cao, L. Xu, and L. Qiao, "The Role of Hydrogen in the Corrosion and Cracking of Steels - A Review," *Corrosion Communications* 4 (2021): 23–32.

16. X. Li, J. Yin, J. Zhang, et al., "Hydrogen Embrittlement and Failure Mechanisms of Multi-Principal Element Alloys: A Review," *Journal of Materials Science and Technology* 122 (2022): 20–32.

17. E. Mokhtari, A. Heidarpour, and F. Javidan, "Mechanical Performance of High Strength Steel Under Corrosion: A Review Study," *Journal of Constructional Steel Research* 220 (2024): 1–23.

18. M. F. Shehata and A. M. El-Shamy, "Hydrogen-Based Failure in Oil and Gas Pipelines a Review," *Gas Science and Engineering.* 115 (2023): 115.

19. Y. Sun and C. Y. Frank, "Hydrogen-Induced Degradation of High-Strength Steel Pipeline Welds: A Critical Review," *Engineering Failure Analysis* 133 (2022): 1–22.

20. Y.-L. Lee, I. Ebrary, and E. Al, *Fatigue Testing and Analysis: Theory and Practice* (Amsterdam; Boston: Elsevier Butterworth-Heinemann, 2005).

21. K. J. Miller and W. J. O'donnell, "The Fatigue Limit and Its Elimination," *Fatigue and Fracture of Engineering Materials and Structures* 22 (1999): 545–557.

22. C. Sonsino, "Course of SN-Curves Especially in the High-Cycle Fatigue Regime With Regard to Component Design and Safety," *International Journal of Fatigue* 29 (2007): 2246–2258.

23. R. C. Rice, W. J. Park, and R. Y. Kim, *Fatigue Data Analysis [1]* (ASM International EBooks, 2000).

24. J. E. Spindel and E. Haibach, "Some Considerations in the Statistical Determination of the Shape of S-N Curves," in *Statistical analysis of fatigue data*, eds. R. E. Little and J. C. Ekvall (ASTM STP 744, 1981): 89–113.

25. R. I. Stephens, A. Fatemi, R. R. Stephens, and H. O. Fuchs, *Metal Fatigue in Engineering* (John Wiley & Sons, 2000).

26. I. Al Zamzami and L. Susmel, "On the Accuracy of Nominal, Structural, and Local Stress Based Approaches in Designing Aluminium Welded Joints Against Fatigue," *International Journal of Fatigue* 101 (2017): 137–158.

27. C. Engler-Pinto, J. V. Lasecki, R. J. Frisch, Sr., D. J. MA, and J. E. Allison, *Statistical Approaches Applied to Fatigue Test Data Analysis, SAE Technical Paper 2005-01-0802* (SAE transactions, 2005).

28. ASTM E739-10, *Standard Practice for Statistical Analysis of Linear or Linearized Stress-Life (S-N) and Strain-Life (ε-N) Fatigue Data, American Society for Test and Materials* (West Conshohocken, PA: ASTM International, 2015).

29. ASTM E3080-19, *Standard Practice for Regression Analysis with a Single Predictor Variable, American Society for Test and Materials* (West Conshohocken, PA: ASTM International, 2019).

30. E. Kufoin and L. Susmel, "Quantitative Review of Probabilistic Approaches to Fatigue Design in the Medium Cycle Fatigue Regime," *Probabilistic Engineering Mechanics* 75 (2024): 103589.

31. R. W. Hertzberg, R. P. Vinci, and J. L. Hertzberg, *Deformation and fracture mechanics of engineering materials* (Wiley, 2020).

32. T. Miyamoto, "Characteristics of Fatigue Life and Fatigue Crack Growth of SCM435 Steel in High-Pressure Hydrogen Gas," *Transactions of the Japan Society of Mechanical Engineers Series A* 78 (2012): 531–546.

33. M. Kubota, Y. Tanaka, and Y. Kondo, "The Effect of Hydrogen Gas Environment on Fretting Fatigue Strength of Materials Used for Hydrogen Utilization Machines," *Tribology International* 42 (2009): 1352–1359.

34. M. H. Kelestemur and T. K. Chaki, "The Effect of Overload on the Fatigue crack Growth Behaviour of 304 Stainless Steel in Hydrogen," *Fatigue and Fracture of Engineering Materials and Structures* 24 (2001): 15–22.

35. T. L. Anderson, *Fracture Mechanics - Fundamentals and Applications*, 4th ed. (Boca Raton, USA: CRC Press, 2017).

36. P. Paris and F. Erdogan, "A Critical Analysis of Crack Propagation Laws," *Journal of Basic Engineering* 85, no. 4 (1963): 528–533.

37. ASTM E647-23a, *Standard Test Method for Measurement of Fatigue Crack Growth Rates, American Society for Test and Materials* (ASTM International, 2023).

38. D. J. Olive, *Linear Regression* (Switzerland: Springer International Publishing, 2017).

39. C. W. San Marchi and B. P. Somerday, *Technical Reference for Hydrogen Compatibility of Materials* (United States: U.S. Department of Energy Office of Scientific and Technical Information, 2012).

40. N. Nagaishi, M. Yoshikawa, S. Okazaki, J. Yamabe, F. Yoshida, and H. Matsunaga, "Evaluation of Fatigue Life and Fatigue Limit of Circumferentially-Notched Type 304 Stainless Steel in Air and Hydrogen Gas Based on Crack-Growth Property and Cyclic Stress-Strain Response," *Engineering Fracture Mechanics* 215 (2019): 164–177.

41. Z. Lin, M. Wang, G. Sun, et al., "The Dependence of Fatigue Property on Applied Stress in X80 Pipeline Steel Notched Specimens in Hydrogen Gas Environment," *International Journal of Fatigue* 183 (2024): 108222.

42. Y. Murakami and S. Matsuoka, "Effect of Hydrogen on Fatigue Crack Growth of Metals," *Engineering Fracture Mechanics* 77 (2010): 1926–1940.

43. I. M. Dmytrakh, R. L. Leshchak, A. M. Syrotyuk, and R. A. Barna, "Effect of Hydrogen Concentration on Fatigue Crack Growth Behaviour in Pipeline Steel," *International Journal of Hydrogen Energy* 42 (2017): 6401–6408.

44. R. Komoda, K. Yamada, M. Kubota, et al., "The Inhibitory Effect of Carbon Monoxide Contained in Hydrogen Gas Environment on Hydrogen-Accelerated Fatigue Crack Growth and Its Loading Frequency Dependency," *International Journal of Hydrogen Energy* 44 (2019): 29007–29016.

45. D. Stalheim, T. Boggess, C. San Marchi, et al., "Microstructure and Mechanical Property Performance of Commercial Grade API Pipeline Steels in High Pressure Gaseous Hydrogen," in *Proceedings of the 2010 8th International Pipeline Conference. 2010 8th International Pipeline Conference*, vol. 2 (ASME, 2010): 529–537.

46. B. Meng, C. Gu, L. Zhang, et al., "Hydrogen Effects on X80 Pipeline Steel in High-Pressure Natural Gas/Hydrogen Mixtures," *International Journal of Hydrogen Energy* 42 (2017): 7404–7412.

47. A. J. Slifka, E. S. Drexler, N. E. Nanninga, et al., "Fatigue Crack Growth of Two Pipeline Steels in a Pressurized Hydrogen Environment," *Corrosion Science* 78 (2014): 313–321.

48. S. Suresh and R. O. Ritchie, "Mechanistic Dissimilarities Between Environmentally Influenced Fatigue-Crack Propagation at Near-Threshold and Higher Growth Rates in Lower Strength Steels," *Metal Science* 16 (1982): 529–538.

49. A. Chandra, R. Thodla, T. J. Prewitt, W. Matthews, and S. Sosa, "Fatigue Crack Growth Study of X70 Line Pipe Steel in Hydrogen Containing Natural Gas Blends," in *Proceedings of the ASME 2021 Pressure Vessels and Piping Conference. Volume 4: Materials and Fabrication. Virtual, Online*, vol. 85345 (American Society of Mechanical Engineers, 2021): V004T06A050.

50. A. Alvaro, D. Wan, V. Olden, and A. Barnoush, "Hydrogen Enhanced Fatigue Crack Growth Rates in a Ferritic Fe-3 wt%Si Alloy and a X70 Pipeline Steel," *Engineering Fracture Mechanics* 219 (2019): 106641.

51. A. Macadre, M. Artamonov, S. Matsuoka, and J. Furtado, "Effects of Hydrogen Pressure and Test Frequency on Fatigue Crack Growth Properties of Ni-Cr-Mo Steel Candidate for a Storage Cylinder of a 70MPa Hydrogen Filling Station," *Engineering Fracture Mechanics* 78 (2011): 3196–3211.

52. V. Di Cocco, E. Franzese, F. Iacoviello, and S. Natali, "22 Cr 5 Ni Duplex and 25 Cr 7 Ni Superduplex Stainless Steel: Hydrogen Influence on Fatigue Crack Propagation Resistance," *Engineering Fracture Mechanics* 75 (2008): 705–714.

53. S. Matsuoka, J. Yamabe, and H. Matsunaga, "Criteria for Determining Hydrogen Compatibility and the Mechanisms for Hydrogen-Assisted, Surface Crack Growth in Austenitic Stainless Steels," *Engineering Fracture Mechanics* 153 (2016): 103–127.

54. Y. Kondo, M. Kubota, and K. Shimada, "Hydrogen Enhanced Crack Propagation of SCM440H Low-Alloy Steel Under Long-Term Varying Load," *Engineering Fracture Mechanics* 77 (2010): 1963–1974.

55. R. Zhang, K. Ma, W. Peng, and J. Zheng, "Effects of Hydrogen Pressure on Hydrogen-Assisted Fatigue Crack Growth of Cr-Mo Steel," *Theoretical and Applied Fracture Mechanics* 129 (2024): 104202.

56. T. Zheng and N. Z. Chen, "A Cyclic Cohesive Zone Model for Predicting Hydrogen Assisted Fatigue Crack Growth (FCG) of Subsea Pipeline Steels," *International Journal of Fatigue* 173 (2023): 107707.

57. C. Zhou, C. Jiang, Y. Jin, et al., "The Regulation of Dislocation and Precipitated Phase Improving Hydrogen Embrittlement Resistance of Pipeline Steel in High Pressure Hydrogen Environment," *International Journal of Fatigue* 190 (2025): 108657.

58. Y. Ogawa, H. Nishida, M. Nakamura, V. Olden, A. Vinogradov, and H. Matsunaga, "Dual Roles of Pearlite Microstructure to Interfere/Facilitate Gaseous Hydrogen-Assisted Fatigue Crack Growth in Plain Carbon Steels," *International Journal of Fatigue* 154 (2022): 106561.

59. L. B. Peral, A. Zafra, S. Blasón, C. Rodríguez, and J. Belzunce, "Effect of Hydrogen on the Fatigue Crack Growth Rate of Quenched and Tempered CrMo and CrMoV Steels," *International Journal of Fatigue* 120 (2019): 201–214.

60. J. Yamabe, M. Yoshikawa, H. Matsunaga, and S. Matsuoka, "Hydrogen Trapping and Fatigue Crack Growth Property of Low-Carbon Steel in Hydrogen-Gas Environment," *International Journal of Fatigue* 102 (2017): 202–213.

61. C. Fischer, S. Fliegener, H. Oesterlin, et al., "Codes and Standards for the Fatigue-Based Design of Hydrogen Infrastructure Components," *International Journal of Fatigue* 171 (2023): 107564.

62. C. Colombo, G. Fumagalli, F. Bolzoni, G. Gobbi, and L. Vergani, "Fatigue Behavior of Hydrogen Pre-Charged Low Alloy Cr-Mo Steel," *International Journal of Fatigue* 83 (2015): 2–9.

63. V. Ramasagara Nagarajan and S. K. Putatunda, "Influence of Dissolved Hydrogen on the Fatigue Crack Growth Behaviour of AISI 4140 Steel," *International Journal of Fatigue* 62 (2014): 236–248.

64. A. Roy, I. Manna, and I. Chattoraj, "Anomalies in Hydrogen Enhanced Fatigue of a High Strength Steel," *International Journal of Fatigue* 59 (2014): 14–22.

65. J. H. Chuang, L. W. Tsay, and C. Chen, "Crack Growth Behaviour of Heat-Treated 4140 Steel in Air and Gaseous Hydrogen," *International Journal of Fatigue* 20 (1998): 531–536.

66. E. S. Drexler, A. J. Slifka, R. L. Amaro, et al., "Fatigue Crack Growth Rates of API X70 Pipeline Steel in a Pressurized Hydrogen Gas Environment," *Fatigue and Fracture of Engineering Materials and Structures* 37 (2014): 517–525.

67. L. W. Tsay and T. Y. Yang, "Reduction of Hydrogen Embrittlement in an Ultra-High-Strength Steel by Laser Surface Annealing," *Fatigue and Fracture of Engineering Materials and Structures* 23 (2000): 325–333.

68. K. Tazoe, S. Hamada, and H. Noguchi, "Fatigue Crack Growth Behavior of JIS SCM440 Steel Near Fatigue Threshold in 9-MPa Hydrogen Gas Environment," *International Journal of Hydrogen Energy* 42 (2017): 13158–13170.

69. C. Zhou, D. Tang, K. Zhang, et al., "Effect of Manganese Content on the Hydrogen Embrittlement of Twinning-Induced Plasticity (TWIP) Steels Under Hydrogen Charging and Hydrogen Environment," *Materials Science and Engineering: A* 861 (2022): 144289.

70. Z. Hua, X. Zhang, J. Zheng, et al., "Hydrogen-Enhanced Fatigue Life Analysis of Cr–Mo Steel High-Pressure Vessels," *International Journal of Hydrogen Energy* 42 (2017): 12005–12014.

71. J. Shang, R. Gao, B. Xing, H. Wei, and Z. Hua, "Enhanced Hydrogen Degradation of Two Pipeline Steels by Increasing Inert Gas Pressure in Hydrogen-Containing Mixtures: Experimental and Theoretical Insights," *Corrosion Science* 240 (2024): 112466.

72. S. Matsuoka, O. Takakuwa, S. Okazaki, M. Yoshikawa, J. Yamabe, and H. Matsunaga, "Peculiar Temperature Dependence of Hydrogen-Enhanced Fatigue Crack Growth Of Low-Carbon Steel in Gaseous Hydrogen," *Scripta Materialia* 154 (2018): 101–105.

73. Y. Ogawa, O. Takakuwa, S. Okazaki, Y. Funakoshi, S. Matsuoka, and H. Matsunaga, "Hydrogen-Assisted Fatigue Crack-Propagation in a Ni-Based Superalloy 718, Revealed via Crack-Path Crystallography and Deformation Microstructures," *Corrosion Science* 174 (2020): 108814.

74. L. Briottet, I. Moro, and P. Lemoine, "Quantifying the Hydrogen Embrittlement of Pipeline Steels for Safety Considerations," *International Journal of Hydrogen Energy* 37 (2012): 17616–17623.

75. Y. S. Ding, L. W. Tsay, and C. Chen, "The Effects of Hydrogen on Fatigue Crack Growth Behaviour of Ti-6Al-4V and Ti-4.5Al-3V-2Mo-2Fe Alloys," *Corrosion Science* 51 (2009): 1413–1419.

76. J. Yamabe, T. Matsumoto, S. Matsuoka, and Y. Murakami, "A New Mechanism in Hydrogen-Enhanced Fatigue Crack Growth Behavior of a 1900-MPa-Class High-Strength Steel," *International Journal of Fracture* 177 (2012): 141–162.

77. L. W. Tsay, M. C. Young, and C. Chen, "Fatigue Crack Growth Behavior of Laser-Processed 304 Stainless Steel in Air and Gaseous Hydrogen," *Corrosion Science* 45 (2003): 1985–1997.

78. J. Shang, W. Chen, J. Zheng, et al., "Enhanced Hydrogen Embrittlement of Low-Carbon Steel to Natural Gas/Hydrogen Mixtures," *Scripta Materialia* 189 (2020): 67–71.

79. S. Wang, A. Nagao, P. Sofronis, and I. M. Robertson, "Hydrogen-Modified Dislocation Structures in a Cyclically Deformed Ferritic-Pearlitic Low Carbon Steel," *Acta Materialia* 144 (2018): 164–176.

80. T. J. Marrow, P. J. Cotterill, and J. E. King, "Temperature Effects on the Mechanism of Time Independent Hydrogen Assisted Fatigue Crack Propagation In Steels," *Acta Metallurgica et Materialia* 40 (1992): 2059–2068.

81. R. Brazill, G. W. Simmons, and R. P. Wei, "Fatigue Crack Growth in 2-1/4-Cr-1Mo Steel Exposed to Hydrogen Containing Gases," *Journal of Engineering Materials and Technology* 101 (1979): 199–204.

82. R. O. Ritchie, S. Suresh, and C. M. Moss, "Near-Threshold Fatigue Crack Growth in 2 1/4 Cr-1Mo Pressure Vessel Steel in Air and Hydrogen," *Journal of Engineering Materials and Technology* 102 (1980): 293–299.

83. S. Fukuyama, "Fatigue Crack Growth of SNCM 439 Steel in High Pressure Hydrogen at Room Temperature," *Journal of the Society of Materials Science, Japan* 34, no. 709 (1984): 714.

84. H. Uyama, Y. Mine, Y. Murakami. Effects of Test Frequency on Fatigue Behaviour in a Tempered Martensitic Steel with Hydrogen Charge 材料 2006 55 726 731 8 https://doi.org/10.2472/jsms.55.726.

85. K. Koide, T. Anraku, A. Iwase, and H. Inoue, "Effect of Hydrogen Partial Pressure on Fatigue Crack Growth Rate of Type304 Stainless Steel in H2/Ar Mixed Gas With Wide Range of Pressures," *ISIJ International* 57 (2017): 1652–1656.

86. G. Lee, D. Bae, and S. Park, "Assessment of the Crack Growth Characteristics at the Low Corrosion Fatigue Limit of an A106 Gr b Steel Pipe Weld," *Metals and Materials International* 16, no. 317 (2010): 321.

87. L. W. Tsay, Y. C. Liu, M. C. Young, and D.-Y. Lin, "Fatigue Crack Growth of AISI 304 Stainless Steel Welds in Air and Hydrogen," *Materials Science and Engineering A* 374 (2004): 204–210.

88. L. W. Tsay, J. J. Chen, and J. C. Huang, "Hydrogen-Assisted Fatigue Crack Growth of AISI 316L Stainless Steel Weld," *Corrosion Science* 50 (2008): 2973–2980.

89. Y.-H. Lee, F. Hui, C. Qiang, et al., "Experimental Research on Fatigue Properties of X80 Pipeline Steel for Synthetic Natural Gas Transmission," *Mathematical Problems in Engineering* 2021 (2021): 1–9.

90. T. An, S. Zhang, M. Feng, et al., "Synergistic Action of Hydrogen Gas and Weld Defects on Fracture Toughness of X80 Pipeline Steel," *International Journal of Fatigue* 120 (2018): 23–32.

91. J. A. Ronevich, E. J. Song, Z. Feng, Y. Wang, C. D'Elia, and M. R. Hill, "Fatigue Crack Growth Rates in High Pressure Hydrogen Gas for Multiple X100 Pipeline Welds Accounting for Crack Location and Residual Stress," *Engineering Fracture Mechanics* 228 (2020): 106846.

92. Y. Murakami and H. Matsunaga, "The Effect of Hydrogen on Fatigue Properties of Steels Used for Fuel Cell System," *International Journal of Fatigue* 28 (2006): 1509–1520.

93. Y. Ogawa, H. Matsunaga, J. Yamabe, M. Yoshikawa, and S. Matsuoka, "Fatigue Limit of Carbon and Cr Mo Steels as a Small Fatigue Crack Threshold in High-Pressure Hydrogen Gas," *International Journal of Hydrogen Energy* 43 (2018): 20133–20142.

94. J.-G. Sezgin and J. Yamabe, "Tensile and Fatigue Properties of 17-4PH Martensitic Stainless Steels in Presence of Hydrogen," *Procedia Structural Integrity* 19 (2019): 249–258.

95. M. Kubota, M. Fukuda, and R. Komoda, "Effect of Hydrogen on Fatigue Limit of SCM435 Low-Alloy Steel," *Procedia Structural Integrity* 19 (2019): 520–527.

96. M. Kubota, T. Nishimura, and Y. Kondo, "Effect of Hydrogen Concentration on Fretting Fatigue Strength," *Journal of Solid Mechanics and Materials Engineering* 4 (2010): 816–829.

97. J. Capelle, J. Gilgert, and G. Pluvinage, "A Fatigue Initiation Parameter for Gas Pipe Steel Submitted to Hydrogen Absorption," *International Journal of Hydrogen Energy* 35 (2010): 833–843.

98. H. Uyama, M. Nakashima, K. Morishige, Y. Mine, and Y. Murakami, "Effects of Hydrogen Charge on Microscopic Fatigue Behaviour of Annealed Carbon Steels," *Fatigue & Fracture of Engineering Materials & Structures* 29 (2006): 1066–1074.

99. M. Kubota, A. Macadre, K. Mori, and R. Mori, "Fatigue Properties of Ultra-Fine Grain Austenitic Stainless Steel and the Effect of Hydrogen. 12th International Fatigue Congress (FATIGUE 2018)," in *MATEC Web of Conf*, vol. 165 (EDP Sciences, 2018): 03007.

100. T. Kanezaki, K. Nagata, H. Matsunaga, and Y. Murakami, "Effects of Hydrogen Charge on Fatigue Strength of Stainless Steels," *Nihon Kikai Gakkai Ronbunshu, A Hen/Transactions of the Japan Society of Mechanical Engineers, Part A* 72 (2006): 106–113.

101. T. Iijima, H. Enoki, J. Yamabe, and B. An, "Effect of High Pressure Gaseous Hydrogen on Fatigue Properties of SUS304 and SUS316 Austenitic Stainless Steel," in *Proceedings of the ASME 2018 Pressure Vessels and Piping Conference. Volume 6B: Materials and Fabrication* (Prague, Czech Republic: ASME, 2018): V06BT06A029.

102. C. San Marchi, J. Yamabe, M. Schwarz, et al., "Global Harmonization of Fatigue Life Testing in Gaseous Hydrogen," in *Proceedings of the ASME 2018 Pressure Vessels and Piping Conference. Volume 6B: Materials and Fabrication* (Prague, Czech Republic: ASME, 2018): V06BT06A041.

103. C. San Marchi and B. P. Somerday, *Technical Reference on Hydrogen Compatibility of Materials*. SANDIA REPORT, SAND2012-7321, (Albuquerque, New Mexico, 87185 and Livermore, California, USA: Sandia National Laboratories, 2012).

104. C.-K. Lin and I.-L. Lan, "Fatigue Behavior of AISI 347 Stainless Steel in Various Environments," *Journal of Materials Science* 39 (2004): 6901–6908.

105. A. Ueno and G. Benjamin, "Effect of High-Pressure H2 Gas on Tensile and Fatigue Properties of Stainless Steel SUS316L by Means of the Internal High-Pressure H2 Gas Method," *Procedia Structural Integrity* 19 (2019): 494–503.

106. Y. Wada, R. Ishigaki, Y. Tanaka, T. Iwadate, and K. Ohnishi, "Evaluation of Metal Materials for Hydrogen Fuel Station," in *Proceedings of the 1992 Annual Meeting of JSME/MMD* (International Conference on Hydrogen Safety, 2005).

107. M. Nagumo, H. Shimura, T. Chaya, H. Hayashi, and I. Ochiai, "Fatigue Damage and Its Interaction With Hydrogen in Martensitic Steels," *Materials Science and Engineering A* 348 (2003): 192–200.

108. H. Wu, S. Hamada, Y. Oda, and H. Noguchi, "Effect of Internal Hydrogen on Very High Cycle Fatigue of Precipitation-Strengthened Steel SUH660," *International Journal of Fatigue* 70 (2015): 406–416.

109. T. Michler, J. Naumann, and E. Sattler, "Influence of High Pressure Gaseous Hydrogen on S-N Fatigue in Two Austenitic Stainless Steels," *International Journal of Fatigue* 51 (2013): 1–7.

110. A. MacAdre, H. Yano, S. Matsuoka, and J. Furtado, "The Effect of Hydrogen on the Fatigue Life of Ni-Cr-Mo Steel Envisaged for Use as a Storage Cylinder for a 70 MPa Hydrogen Station," *International Journal of Fatigue* 33 (2011): 1608–1619.

111. M. H. M. Kouters, H. M. Slot, W. Van Zwieten, and J. Van Der Veer, "The Influence of Hydrogen on the Fatigue Life of Metallic Leaf Spring Components in a Vacuum Environment," *International Journal of Fatigue* 59 (2014): 309–314.

112. H. Li, F. Dong, Q. Zhou, et al., "Influence of Hydrogen on the S–N Fatigue of DP1180 Advanced High-Strength Steel," *Corrosion Science* 205 (2022): 110465.

113. T. Michler, J. Naumann, S. Weber, M. Martin, and R. Pargeter, "S-N Fatigue Properties of a Stable High-Aluminum Austenitic Stainless Steel for Hydrogen Applications," *International Journal of Hydrogen Energy* 38 (2013): 9935–9941.

114. M. Nakatani and K. Minoshima, "Influence of Activation Energy and Sensitivity to Hydrogen Embrittlement on Fatigue Strength Degradation by Irreversible Hydrogen in High-Strength Steels," *Fatigue and Fracture of Engineering Materials and Structures* 34 (2011): 363–373.

115. M. Okayasu and H. Matsuura, "Hydrogen Embrittlement Properties of Several Stainless Steels," *International Journal of Fracture* 248 (2024): 201–220.

116. S. Rahimi, A. M. De Jesus, D. Meng, et al., "Very High-Cycle Fatigue Behavior of Steel in Hydrogen Environment: State of the Art Review and Challenges," *Engineering Failure Analysis* 166 (2024): 108898.